# Size-fractioned zooplankton biomass in the Barents Sea: Spatial patterns and temporal variations during three decades of warming and strong fluctuations of the capelin stock (1989–2020)

Hein Rune Skjoldal [*], Elena Eriksen, Harald Gjøsæter

*Institute of Marine Research, P.O. Box 1870 Nordnes, NO-5817 Bergen, Norway*

## ARTICLE INFO

## ABSTRACT

Zooplankton biomass has been monitored on joint Norwegian-Russian surveys in late summer and autumn since the 1980s. We report here on zooplankton biomass in three size fractions ($<1$, 1–2, and $>2$ mm in screen mesh opening) obtained with WP-2 plankton net (180 μm mesh size) hauled vertically over the water column from near bottom to the surface for the period 1989–2020. The number of samples (stations) collected each year has been about 100–200, with a total number of 4543 stations for the whole data set. The size composition of zooplankton reflected by the three fractions has shown remarkable stability, with about 50% of biomass contained in the medium fraction (made up largely of *Calanus* species), about 1/3 in the small fraction (36%), and 16% in the large fraction. The depth integrated biomass was generally larger in basins compared to shallower bank areas. The temporal (interannual) pattern of change was characterized by a marked peak in biomass in 1994 and 1995 with values up to $>20$ g dry weight (dw) m$^{-2}$, driven to large extent by the small size fraction. Subsequently the biomass decreased to lower values but with a divergence of relatively high values (10–15 g dw m$^{-2}$) in the inflow area of Atlantic water in southwest, and low values (2–6 g dw m$^{-2}$) in the central area. The difference is interpreted to reflect an increase in a second summer generation of *Calanus finmarchicus* in the Atlantic water and a decrease of *C. glacialis* in the central area. The zooplankton biomass fluctuated inversely with the biomass of the Barents Sea capelin (*Mallotus villosus*) stock, reflecting a top-down predation effect. However, biomass was also negatively correlated with temperature of the Atlantic water, suggesting an additional and confounding effect of climate variability and change. The decrease in biomass of the central area used as a forage area by capelin, was associated with a shift to dominance by the small size fraction. This is likely an effect of predation and could be associated with a lower trophic conversion efficiency from phytoplankton to planktivorous fish and higher trophic levels by smaller zooplankton (smaller copepods such as *Pseudocalanus* and others) compared to the larger *Calanus* species.

## 1. Introduction

The Barents Sea is a globally unique ecosystem stemming from its high-latitude position (roughly between 70 and 80°N). It is a relatively deep shelf sea (mean depth 240 m) situated on the northwestern corner of the Eurasian tectonic plate. It lies about half-way into the Arctic Mediterranean Sea, the sea area north of the Scotland-Greenland Ridge (Rudels, 2021, Eldevik et al., 2021), and forms an important part of what is termed the Atlantic Gateway to the Arctic Ocean (Drinkwater et al., 2021, Ingvaldsen et al., 2021, Skjoldal, 2022). Relatively warm Atlantic water as a branch from the Gulf Stream flows north along Norway and

splits at the southwestern entrance into two branches, one flowing around, and the other flowing into and across the Barents Sea shelf. The former is the West-Spitsbergen Current and the latter the North Cape Current (Skagseth et al., 2008).

The Atlantic water from the North Cape Current flows east through the southern Barents Sea and then north through the eastern part of the sea towards the northeastern exit between Novaya Zemlya and Franz Josef Land (Fig. 1). A smaller branch of Atlantic water splits off in the Bear Island Trench and flows north in the Hopen Deep and then turn east in the depression between the Central Bank and the Great Bank. The Atlantic water is cooled on its way from the Barents Sea Opening (BSO)

---

in south-west to the Barents Sea Exit in north-east by about 4–5 °C, to around 0 °C for the exiting water (Skagseth et al., 2020). This flow pattern and the cooling of the Atlantic water give a strong flow-through character to the Barents Sea ecosystem and determine it as a broad biogeographical transition zone between the boreal and Arctic bio-climatic zones. These features are particularly important for plankton, which drift with the currents, compared with more resident benthos and migratory fish.

Two species of *Calanus* copepods play dominant roles in the Barents Sea ecosystem where they make up about 70% of the total meso-zooplankton biomass (Aarflot et al., 2018b). *Calanus finmarchicus* is a boreal species with core habitat in the deep basins of the subpolar gyres in the Norwegian and Labrador seas at temperatures of about 5–10 °C (Conover, 1988, Sundby, 2000, Helaouët and Beaugrand, 2007, Helaouët et al., 2011, Melle et al., 2014). It is transported with the Atlantic water from the Norwegian Sea into the Barents Sea where it is the dominant copepod along the transport route of the Atlantic water in the southern and eastern parts. *C. finmarchicus* reproduces in spring with egg production closely related to the early phase of the spring growth of phytoplankton (Tande, 1991, Melle and Skjoldal, 1998). It produces one distinct annual cohort as a spring-summer generation G1 which peaks in

numerical abundance typically in June (Skjoldal, 2021, Skjoldal et al., 1987). Due to the strong increase in size (weight) of the individuals, the total biomass of *C. finmarchicus* is reflecting mainly the older copepodite stages, CIV, CV and adults (Aarflot et al., 2018b). The seasonal build-up of biomass of *C. finmarchicus* is therefore delayed compared to numbers, and the peak in biomass is broader, lasting as a feature from summer into autumn (Aarflot et al., 2018b, see their Fig. 8).

Generations of *Calanus finmarchicus* develop with a spatial pattern in the flow direction of Atlantic water into and through the Barents Sea. Because the overwintering generation resides deep (mainly below 600 m) in the Norwegian Sea (Østvedt, 1955, Melle et al., 2004, Edvardsen et al., 2006), the Atlantic water that flows into the Barents Sea in winter contains few *C. finmarchicus* (Skjoldal, 2021, Skjoldal et al., 1992). As the overwintering generation (G0) ascends in late winter, a spring generation (G1) develops in the inflow region to the Barents Sea with a peak around June (Degtereva, 1979, Dalpadado et al., 2012, 2020, Kvile et al., 2014). At the same time, a G1 is developing based on spawning by overwintering (G0) inside the Barents Sea, stemming from a generation (G1, and possibly G2) transported into the Barents Sea the year before (Melle and Skjoldal, 1998, Kvile et al., 2017). There is growing evidence that a second, summer generation (G2) of *C. finmarchicus* develops in the
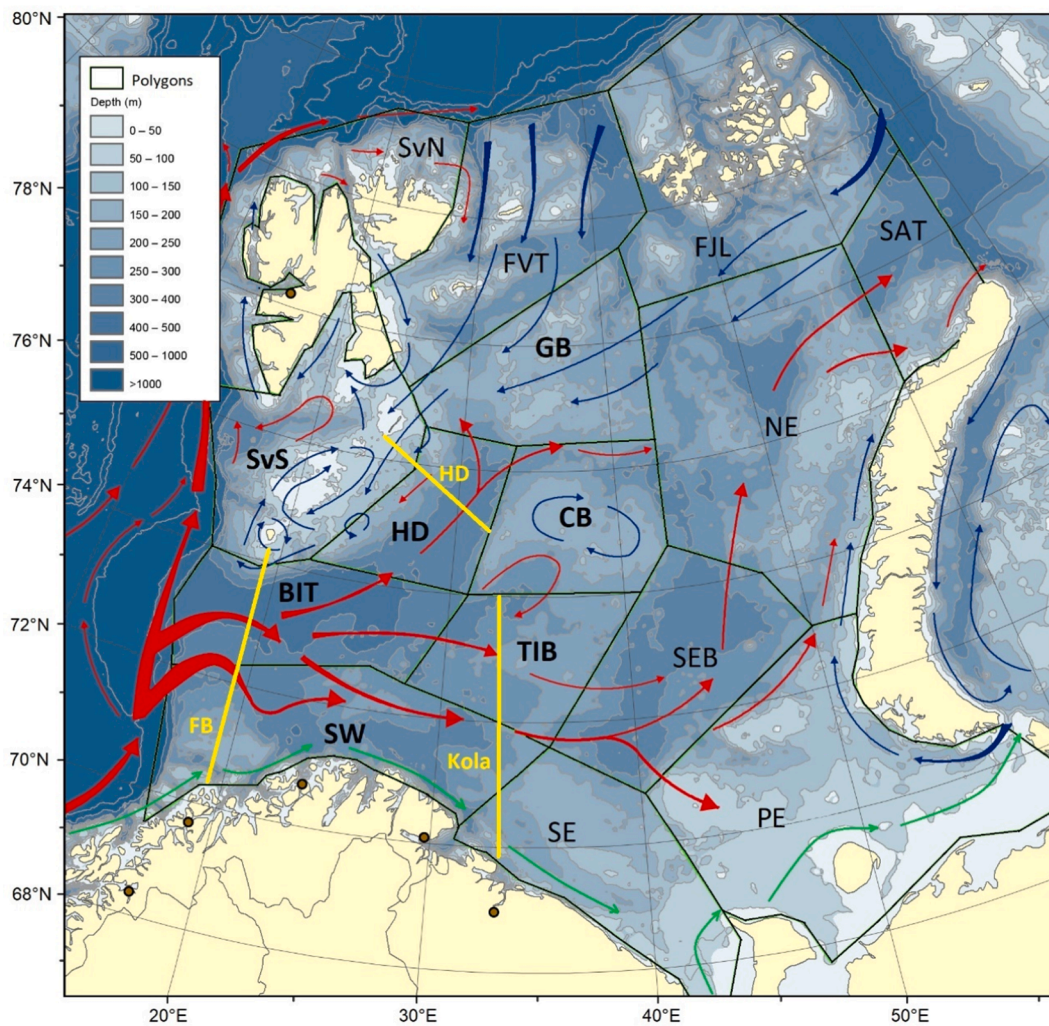


**Fig. 1.** Map of the Barents Sea with bottom topography and ocean currents shown as arrows: green – coastal currents, red – Atlantic water currents, blue – Arctic water currents. Black lines show delineation of fifteen subareas or polygons (see Material and methods). Yellow lines show positions of the Fugløya-Bear Island (FB, or Barents Sea Opening BSO) and Kola oceanographic transects. Abbreviations of polygon names used in the text: BIT – Bear Island Trench, CB – Central Bank, FJL – Franz Josef Land, FVT – Franz-Victoria Trough, GB – Great Bank, HD – Hopen Deep, NE – North-East, PE – Pechora, SAT – St. Anna Trough, SE – South-East, SEB – Southeastern Basin, SvN – Svalbard North, SvS – Svalbard South, SW – South-West. Seven selected polygons used to describe temporal patterns are located in the western and central Barents Sea: SW, BIT, TIB, HD, CB, GB, and SvS.

Atlantic water in the inflow region to the Barents Sea between June and August (Gluchowska et al., 2017, Strand et al., 2020, Skjoldal et al., 2021).

The transport across the BSO is complex and dynamic but with relatively low net current speed of 2–4 cm s$^{-1}$ into the Barents Sea (Ingvaldsen et al., 2004). At these speeds, a generation of *C. finmarchicus* would be transported 200–400 km during a four-month period between May and September. This would bring external G1 and G2 generations from the BSO toward the central Barents Sea, while an internal G1 formed in the central Barents Sea would be transported toward the eastern Barents Sea. With the cooling of the Atlantic water as it is transported north through the eastern Barents Sea, the generations of *C. finmarchicus* develop more slowly and are eventually expatriated, unable to reproduce successfully (Melle and Skjoldal, 1998, Hirche and Kosobokova, 2007, Ji et al., 2012, Tarling et al., 2022).

The second dominant *Calanus* species, *Calanus glacialis*, is an Arctic sibling species of *C. finmarchicus*, distributed in the cold, Arctic water mass of the northern Barents Sea (Tande, 1991). *C. glacialis* is larger (weighs about three times more than C. *finmarchicus*) and may have a two-year life cycle in ice-covered Arctic waters (Conover, 1988, Melle and Skjoldal, 1998, Falk-Petersen et al., 2009, Søreide et al., 2010, Daase et al., 2013). The Arctic water mass is generated by cycles of ice formation and ice melt, which leads to a general stratification of the water column. The Arctic water floats as a 'blanket' about 100 m thick on top of Atlantic or modified Atlantic water (Lind and Ingvaldsen, 2012, Lind et al., 2016). The Arctic water layer is seasonally dynamic; it cools to freezing temperature and homogenizes from brine excretion associated with ice formation in winter and stratifies in summer with a thin layer of melt water (10–20 m thick) overlying a core of cold Arctic winter water (Rudels, 1989, Loeng, 1991). The flow pattern of the Arctic water is in southwestern direction as the broad Persey Current in the northern Barents Sea, continuing as the Bear Island Current along the Spitsbergen Bank and up along western Spitsbergen (Fig. 1; Ozhigin et al., 2011). There are probably clockwise circulation patterns of Arctic water around the Svalbard and Franz Josef Land archipelagoes, which give some degree of containment of the *C. glacialis* population to the waters of the northern Barents Sea.

The two *Calanus* species co-occur in wide areas of the central Barents Sea where Atlantic and Arctic water masses meet and mix. Through vertical migration, e.g., between deeper Atlantic and upper Arctic water layers, the copepods can co-occur even if there is limited physical mixing of water masses. With the ongoing warming, the properties and boundaries of the water masses have changed. The Barents Sea has warmed by nearly 2 °C since 1980, and there has been a nearly synchronous increase in temperature in all parts of the Barents Sea (Dalpadado et al., 2020, Skagseth et al., 2020). With the warming, we expect there has been an expansion of favorable habitat for *Calanus finmarchicus* further east and north in the flow-branches of Atlantic water (Dalpadado et al., 2014, 2020). At the same time, the habitat for *Calanus glacialis* has probably shrunk, most notably in the southern extent of the Arctic water such as over the Central Bank. This bank area has a central position and a central role in the Barents Sea by splitting the Atlantic inflow into two branches (Fig. 1). It used to be covered by sea ice in winter and to have an Arctic water mass rotating clockwise as a resident oceanographic feature (Quadfasel et al., 1992). The sea ice has declined in concert with the warming, and the maximum sea ice in winter (March) has declined by about 0.4 million km$^2$, or about 50%, as a linear trend since 1980 (Onarheim et al., 2018). In recent warm years, the Central Bank has not been ice-covered and cold Arctic water is no longer present on the bank.

The warming has proceeded with an oscillatory pattern, driven to a large extent by the variable inflow and increased heat content of Atlantic water (Skagseth et al., 2020, Ingvaldsen et al., 2021, Smedsrud et al., 2022). The dominant influence of Atlantic water is reflected in a coherent and synchronous pattern of temperature variations in different parts of the Barents Sea (Skagseth et al., 2020). The temperature of the

Atlantic water at the Russian Kola section is a climate series which reflects well the overall changes in temperature conditions of the Barents Sea (Dippner and Ottersen, 2001, Ottersen and Stenseth, 2001, Ingvaldsen et al., 2003). The Kola temperature has shown a nearly 2 °C increase between a minimum in 1997 (3.5 °C) and a maximum in 2012 (5.4 °C) (Fig. 2).

Zooplankton has been monitored in the Barents Sea by the Institute of Marine Research in Norway with a standardized procedure since the late 1980s. The procedure includes determination of zooplankton biomass (as dry weight) in three size fractions, as a trait-based (size) approach (Skjoldal, 2021, Skjoldal et al., 2013). We report here on results from the monitoring of zooplankton biomass for the 1989–2020 period, spanning now more than three decades of general warming. Data for the total zooplankton biomass (sum of the three fractions) for the period 1989–2017 was presented by Dalpadado et al. (2020) along with data on phytoplankton primary production estimated from satellite remote sensing of chlorophyll. Stige et al. (2014) used the data on biomass of size fractions up to 2010 to demonstrate strong inverse relationship between zooplankton biomass and biomass of planktivorous fishes, which suggested top-down control of zooplankton by fish predation. This had previously been suggested based on shorter time series of zooplankton biomass data from the Barents Sea (Skjoldal et al., 1992, Dalpadado et al., 2002, 2003, Gjøsæter et al., 2002).

Capelin is the dominant planktivorous fish in the Barents Sea and a key species in the ecosystem (Skjoldal and Rey, 1989, Wassmann et al., 2006, Hop and Gjøsæter, 2013, Hunt et al., 2013, Stige et al., 2014, Eriksen et al., 2017). It is a migratory species that moves from overwintering in the polar front region of the central Barents Sea into the cold Arctic waters on a seasonal feeding migration (Ozhigin and Luka, 1985, Sakshaug and Skjoldal, 1989, Giske et al., 1998, Huse and Ellingsen, 2008). The Barents Sea capelin has shown dramatic fluctuations in stock size, with four collapses and subsequent rapid recoveries, with roughly a decadal pattern (Fig. 2; Skjoldal et al., 1992, Gjøsæter et al., 2009). Zooplankton biomass has fluctuated in an opposite manner to capelin, being lower when capelin is high and vice versa. This is interpreted to reflect top-down predation impact and regulation by capelin on the zooplankton stock (Stige et al., 2014, Dalpadado et al., 2020). Strong inverse relationship consistent with predation impact was observed for capelin versus two krill species (Dalpadado and Skjoldal, 1996). A dedicated two-ship study in August 1985 demonstrated strong predation impact on zooplankton by the migratory 'capelin front' (Hassel et al., 1991). Other important planktivorous fishes in the Barents Sea are polar cod (*Boreogadus saida*) distributed in the cold waters of the eastern and northern parts, and juvenile Atlantic herring (*Clupea harengus*) distributed in the warmer Atlantic water of the southern Barents Sea (Eriksen et al., 2017). In addition, pelagically distributed juveniles of many fish species including Atlantic cod (*Gadus morhua*) and haddock (*Melanogrammus aeglefinus*) contribute importantly as planktivores in the summer and autumn seasons (Eriksen et al., 2011, 2017).

We report here on spatial and temporal patterns of size-fractioned zooplankton biomass in the Barents Sea over the last three decades (32 years, 1989–2020) with data from standardized surveys in autumn. The Barents Sea is divided into 15 subareas or 'polygons' based on topography and oceanography (Fig. 1; WGIBAR, 2017), which have been used to examine spatial patterns and perform ecological synthesis across data sets for various ecosystem components (e.g., Dalpadado et al., 2020, Eriksen et al., 2020, Skagseth et al., 2020). We use this division of polygons in our study, with annual values of mean zooplankton biomass for polygons as the primary data units. The zooplankton data set is large (a total of 4543 sampling stations) and is most complete for the western (Norwegian) part of the Barents Sea, which is the focal area for analysis of temporal changes over the full length of the time series. The data set also includes the eastern part (with most samples from the 1990s), which we use to characterize spatial patterns over the whole Barents Sea. Specifically, we examine temporal and spatial changes in zooplankton biomass of three size fractions and
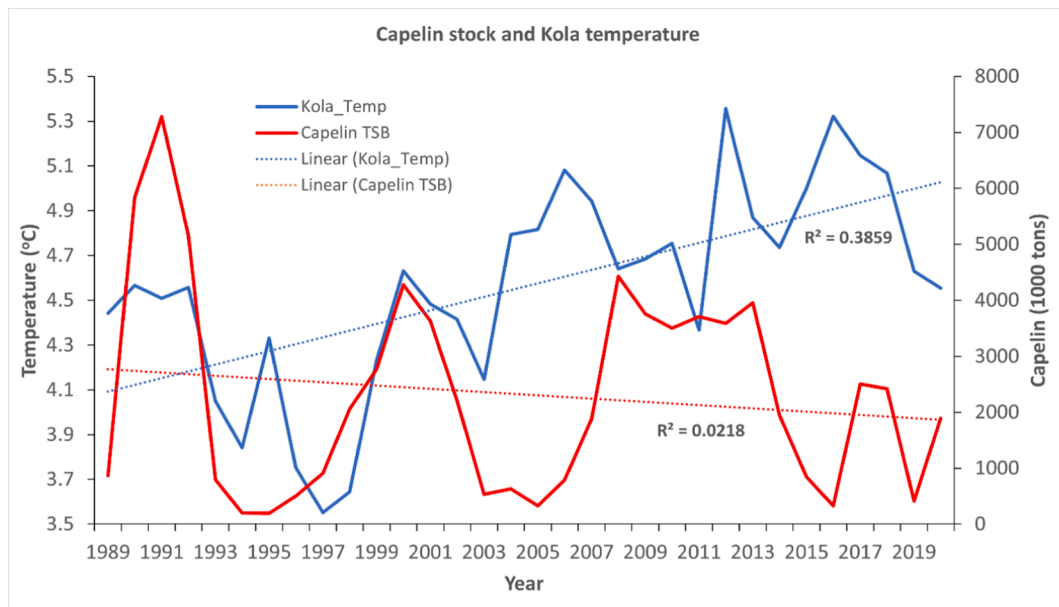
**Fig. 2.** Annual mean temperature of Atlantic water at the Russian Kola section and total stock biomass (TSB) of capelin from 1989 to 2020. Linear trendlines are shown, which are statistically significant for temperature but not for capelin.

their sum in relation to the temperature fluctuations and general warming over the study period, and to the pronounced fluctuations of the caplin stock representing the major planktivorous fish in the Barents Sea. We use the general information on the two dominant *Calanus* species as background for interpreting observed changes in zooplankton biomass in relation to warming and predation from capelin.

## 2. Material and methods

### 2.1. Joint Norwegian-Russian autumn surveys

The data presented in this paper were collected on joint Norwegian-Russian autumn surveys in the Barents Sea in 1989–2020, carried out by the Institute of Marine Research (IMR) in Norway and the Polar Branch of Russian Federal Research Institute of Fisheries and Oceanography (PINRO) in Murmansk, Russia. The joint surveys started out as separate 0-group fish and capelin acoustic surveys in the 1960s and 1970s and were expanded as a multispecies survey from the mid-1980s and as an ecosystem survey from 2003 (Eriksen et al., 2018). The surveys have been conducted with 4–5 research vessels and have typically started around mid-August and lasted through September into early October. The area covered by the survey is large (of order 1 million km$^2$), and even with multiple ships, it takes about 6 weeks to complete the semi-synoptic mapping of environmental conditions, fish stocks and other biological components. There has been a northward expansion of the survey area in concert with reduction in sea ice and northward displacement of biota in the recent decades (Michalsen et al., 2013, Ingvaldsen et al., 2021).

### 2.2. Zooplankton sampling

In the joint sampling program with PINRO, IMR has sampled zooplankton in the Barents Sea with two different nets: WP-2 and MOCNESS multinet sampler. We are here reporting only on the IMR data obtained with WP-2 net. The WP-2 net is conical with net opening of 0.25-m$^2$ and used with 180 μm mesh plankton gauze (Tranter, 1968, Skjoldal et al., 2019). The net is operated with vertical hauls from near the bottom (about 10 m above) to the surface. It is used without flowmeter, and the volume of water filtered through the net is calculated from tow length and net opening (Skjoldal et al., 2019).

### 2.3. Determination of biomass

The biomass as dry weight of zooplankton was determined according to the standard method used at IMR since the mid-1980s (Hassel et al., 2020). The cod-end with the zooplankton sample from a net is put into a tray and any large gelatinous plankton are picked out and removed from the sample (recorded separately) in order not to interfere with the size fractionation. The sample is then divided in two halves with a Motoda plankton splitter. One half-sample for analysis of taxonomic composition is preserved with formaldehyde and stored, while the other half is used for determination of dry weight biomass in three size fractions by successive wet sieving through screens with 2,000, 1,000, and 180 μm mesh size. The contents retained on these three screens are transferred to pre-weighed aluminum trays and weighed after drying. For more details on the method, see e.g., Skjoldal et al. (2013).

We denote the three fractions retained on the three screens as the large, medium, and small fractions, characterized by size > 2 mm, 1–2 mm, and < 1 mm, respectively. Note that these sizes refer to the mesh size of the screens, and not directly to the size of the zooplankton individuals. However, there is a fairly strict relationship between size of copepods and the fractions they are being separated into (Skjoldal, 2021). Thus, small copepods like the numerically dominant *Oithona*, *Microcalanus*, and *Pseudocalanus* species are contained in the small fraction, as are the young copepodite stages CI-CIII of the two dominant *Calanus* species, *C. finmarchicus* and *C. glacialis*. Stage CIV of the two *Calanus* species are split about 50–50 between the small and medium fractions, while the older copepodites CV and adults are contained mainly in the medium fraction. The small fraction contains in addition to small copepods, also meroplanktonic larvae (bivalves, polychaetes, echinoderms and others) and small individuals of appendicularians. The large fraction contains large individuals of copepods (*Calanus hyperboreus*, *Paraeuchaeta* spp.), chaetognaths, hyperiid amphipods, and krill species (Skjoldal, 2021).

### 2.4. Data set

The data set reported here included a total of 4543 stations with a single WP-2 net haul at each station. The number of stations each year varied from 77 to 197, with an average of 142 stations. The biomass of zooplankton is depth-integrated over the whole water column (except

for the ~ 10 m thick layer above the seafloor) and expressed in units of g dry weight (dw) m$^{-2}$.

For the purpose of integrated data analyses, the Barents Sea has been divided into 15 subareas or polygons (Fig. 1; WGIBAR, 2017). The division is based broadly on topography and oceanography, with polygons dominated by either shallow banks or deeper troughs or depressions. The number of zooplankton sampling stations in each of the polygons are summarized in Table S-1. For seven polygons in the western and central Barents Sea, the coverage is relatively good in all years, with on average 12–23 stations per polygon. These polygons are South-West (SW), Bear Island Trench (BIT), Thor Iversen Bank (TIB), Hopen Deep (HD), Central Bank (CB), Great Bank (GB), and Svalbard-South (SvS) (Fig. 1). For the Franz-Victoria Trench (FVT) polygon, the coverage is also relatively good (average 10 stations per year) but with low number of stations some years (Table S-1).

Reflecting the northward expansion of the coverage, the Svalbard-North (SvN) polygon has been relatively well covered since 2009. IMR ships covered some of the polygons in the eastern Barents Sea (South-East – SE, Pechora – PE, North-East – NE) during the 1990s but with few or no samples in recent decades. The two most northeastern polygons (Franz Josef Land – FJL, and St. Anna Trough – SAT) were covered with only a few stations in the 1990s. The Southeastern Basin (SEB) polygon has been sampled in most years, but with few stations per year after year 2000 (Table S-1).

The primary data units used in this study are annual polygon means of zooplankton biomass calculated as the arithmetic mean values of biomass in each of the three fractions and total (sum of fractions). The data are summarized including standard deviation (SD) and number of observations (stations) for each polygon and year in Tables S-2 – S-15. The data on zooplankton biomass follow log-normal distributions (Skjoldal, unpublished results), and log-transformation of the data might be more correct for describing the variance. However, linear arithmetic averaging is the most appropriate for estimating the spatially integrated zooplankton biomass, and the mean values and associated SD are therefore used to characterize the primary data.

### 2.5. Explanatory variables

We examined relationships with stock size of the Barents Sea capelin and various climate indices as explanatory variables for patterns of change in zooplankton biomass.

The capelin stock size as biomass is estimated as the sum of the immature and maturing parts of the stock. The annual estimates stem from capelin investigations carried out during the same surveys as the zooplankton measurements and were taken from the capelin stock assessments carried out by the International Council for the Exploration of the Sea (ICES; AFWG, 2021).

Temperature of the Atlantic water at the Kola section (along the 33.5°E longitude) averaged for the 0–200 m depth layer between 70.5 and 72.5°N was used as a temperature index representative of the temperature fluctuations in the inflowing Atlantic water in the Barents Sea (Ottersen and Stenseth, 2001, Ingvaldsen et al., 2003). The corresponding salinity at the Kola section was used as an additional variable. We also used three expressions of areal extent (distribution) of water masses defined by temperature: Atlantic water (>3 °C), mixed water (0–3 °C), and Arctic water (<0 °C). The areas are calculated based on average temperature for the 50–200 m depth interval for sampling stations at the same autumn surveys where the zooplankton data are collected (Johannesen et al., 2012). Finally, we used the North Atlantic Oscillation (NAO) winter index (November-March) as an additional climate index related to wind conditions and variable inflow of water to the Barents Sea (e.g., Ådlandsvik and Loeng, 1991). The data for the climate indices series (1989–2020) were obtained from WGIBAR (2021).

### 2.6. Multivariate and statistical analyses

Analysis of variance (ANOVA) – ANOVA was used to describe variation of zooplankton biomass with time (years) and in space (between polygons). Two-ways ANOVA without replication (using polygon mean values) was done with Microsoft Excel for the sets of biomasses of each size fraction and total, 1989–2020.

Principal Component Analysis (PCA) – PCA was performed to explore patterns of spatial–temporal variation in the zooplankton biomass data sets made up of annual polygon mean values. A PCA was run with the four variables of zooplankton biomass (fractions and total) across all polygons and years (304 data lines of combinations of polygons and years, giving a 4 × 304 matrix). Two PCAs were run with the time series of seven selected polygons (with good data coverage, see section Data set) as separate variables across the years. One version was run with the total biomass (7 variables, one for each polygon) in a 7 × 32 (years) matrix. A second version was run with the three size fractions for each of the seven polygons in a 21 × 32 matrix (3 fractions times 7 polygons and 32 years). PCA was performed using PAST 3.14 (Hammer et al., 2001) with data standardized to zero mean and unit variance.

Non-metric multidimensional scaling (NMDS) – An NMDS analysis was run with a data set of zooplankton biomass (three fractions and total) for the seven selected polygons over 32 years (1989–2020) using capelin stock size (maturing part and total) and climate indices (see section Explanatory variables) as additional variables. NMDS was performed using PAST 3.14 (Hammer et al., 2001) with Bray-Curtis similarity index.

Correlations and linear trends – Ordinary (Pearson product-moment) correlation coefficient (r) was used to explore and indicate strength of relationships between variations of zooplankton biomass of the three fractions and total across polygons and in relation to variations of capelin stock size and climate variables. R$^2$ (Pearson r squared) was used to indicate fraction of variance explained by a linear trend in bivariate relationships. Statistical significance of correlations was indicated by the t-statistic. In our case with data series over 32 years, the critical r values at the 5% and 1% probability levels are 0.30 and 0.41, respectively. These values are on the low side since the effects of multiple comparisons and autocorrelation in the time series have not been accounted for. The non-parametric Mann-Kendall trend test was used to identify statistically significant trends in zooplankton biomass with time.

Multivariate multiple linear regression (MMLR) – MMLR was performed (using PAST 3.14, Hammer et al., 2001) with three measures of zooplankton biomass as dependent variables and capelin stock size (total stock biomass) and Kola temperature (as a climate index) as independent (explanatory) variables. The three measures of zooplankton biomass were the first principal component from the two PCAs for the seven polygons (total biomass and biomass of the three fractions, respectively), and the average total biomass for the seven polygons.

## 3. Results

### 3.1. Polygon means and variability

The zooplankton sampling stations within a polygon (Fig. 1) each year were used to calculate a set of annual polygon-mean values of biomass in the three fractions and total. The number of sampling stations used to estimate the annual polygon means varied from one to 40, with an average of 13 (Table 1). Excluding polygons with only one or two stations (23 and 13 cases representing 49 stations), the statistics of the polygon means over all polygons and years are summarized in Table 1. The total mesozooplankton biomass was 7.2 g dw m$^{-2}$ as an overall average, varying from a minimum of 0.8 to a maximum of 23 g dw m$^{-2}$.

The variation across all the annual polygon-mean values (n = 306–308), expressed as coefficient of variation (CoV = SD/mean), was somewhat larger for the large fraction (0.72) compared to the medium and small fractions (0.59, 0.58), and smallest for the total (0.47;

**Table 1**

Statistical summary of data as polygon-mean biomass values in the three size fractions and total, and number of stations n used to calculate each polygon mean biomass value. The total number of stations is 4543. SD – standard deviation, CoV – coefficient of variation (=SD/mean). 'CoV – stations' are the average CoV values for the variation among the stations used to calculate an annual polygon mean. Min and max are minimum and maximum values. '%' is the overall average biomass composition of the three fractions based on the mean values.

| | | Biomass (g dw m$^{-2}$) | | | |
|---|---|---|---|---|---|
| | n stations | Large | Medium | Small | Total |
| Mean | 13.1 | 1.17 | 3.46 | 2.58 | 7.17 |
| SD | 8.0 | 0.84 | 2.03 | 1.50 | 3.40 |
| CoV | | 0.72 | 0.59 | 0.58 | 0.47 |
| CoV - stations | | 1.11 | 0.82 | 0.58 | 0.61 |
| Median | 13 | 0.99 | 3.21 | 2.25 | 6.86 |
| Min | 1 | 0 | 0 | 0.22 | 0.75 |
| Max | 40 | 4.96 | 12.54 | 10.37 | 23.18 |
| n | | 306 | 307 | 307 | 308 |
| % | | 16.2 | 48.0 | 35.8 | 100 |

Table 1). The variation among the stations used to calculate the annual polygon mean values was somewhat higher (1.1 and 0.82 for the large and medium fractions, and 0.61 for the total biomass; Table 1). The frequency distributions of individual CoV values (for each polygon and year) were skewed to higher values for the large fraction compared to the medium fraction, and for the medium fraction compared to the small fraction (Fig. S-1). The distribution of CoV values for the total biomass was more 'compact' and comparable to the small fraction, reflecting that the higher variability for the large and medium fractions was dampened when the fractions were summed.

### 3.2. Relationships between the size fractions

Nearly half the biomass (48%) was on average found in the medium size fraction, with 36% in the small and 16% in the large fractions (Table 1). The three fractions were positively correlated with the total biomass (Table 2). While they are not independent (since the total is the sum of the fractions), this demonstrates that each fraction contributed positively to an increase in the total biomass. The medium fraction was strongly correlated with the total ($R^2 = 0.81$). The positive correlations with the total biomass were reflected in positive correlations between the fractions. The lowest correlation was between the large and small fractions. A PCA showed a contrasting pattern between the small fraction on one hand and the large fraction on the other, separated along the second axis (PC2; Fig. S-2).

### 3.3. Variation in space (polygons) and time (years) – ANOVA

A two-way ANOVA was performed on the annual polygon mean zooplankton biomass values for seven of the polygons in the western and central Barents Sea which had coverage over the whole time series (Table S-1). The variation across years and polygons was statistically highly significant (p $<10^{-5}$) for all fractions and the total, with the lowest relative variance for the variation among polygons for the smallest fraction (Table 3).

**Table 2**

Correlation coefficients (Pearson r) for the variation in zooplankton in three size fractions and total (sum of fractions) for annual mean polygon values across all polygons and years (1989–2020). Bold indicates statistical significance at p < 0.001 level, while italics indicate significance at p < 0.05.

| | Large | Medium | Small |
|---|---|---|---|
| Medium | **0.46** | | |
| Small | *0.15* | **0.39** | |
| Total | **0.60** | **0.90** | **0.69** |

**Table 3**

Results from two-ways ANOVA (without replication) for the effects of years (1989–2020) and polygons (seven – SW, BIT, TIB, HD, CB, GB, SvS) for variation of zooplankton biomass in three size fractions and total (sum of fractions). SS – sum of squares, df – degrees of freedom, MS – mean sum of squares, F – F statistic, p – probability level for statistically significant effect.

| Fraction | Source of Variation | SS | df | MS | F | p |
|---|---|---|---|---|---|---|
| Large | Year | 48.6 | 31 | 1.57 | 6.25 | 3.37E-16 |
| | Polygon | 37.3 | 6 | 6.22 | 24.77 | 1.72E-21 |
| | Error | 46.7 | 186 | 0.25 | | |
| | Total | 132.6 | 223 | | | |
| Medium | Year | 204.7 | 31 | 6.60 | 3.88 | 4E-09 |
| | Polygon | 351.6 | 6 | 58.60 | 34.43 | 8.48E-28 |
| | Error | 316.5 | 186 | 1.70 | | |
| | Total | 872.8 | 223 | | | |
| Small | Year | 189.1 | 31 | 6.10 | 4.82 | 5.07E-12 |
| | Polygon | 50.2 | 6 | 8.36 | 6.60 | 2.42E-06 |
| | Error | 235.5 | 186 | 1.27 | | |
| | Total | 474.8 | 223 | | | |
| Total | Year | 784.0 | 31 | 25.29 | 5.61 | 2.25E-14 |
| | Polygon | 882.6 | 6 | 147.09 | 32.63 | 1.09E-26 |
| | Error | 838.6 | 186 | 4.51 | | |
| | Total | 2505.2 | 223 | | | |

### 3.4. Spatial patterns

The average total zooplankton biomass varied by a factor of 3 across the polygons, from a low of 3.5 g dw m$^{-2}$ (PE) to a high of about 11 g dw m$^{-2}$ (BIT) (Fig. 3A). There was a pattern of higher biomass (integrated over the water column) for the deeper polygons (BIT, HD, SEB) and lower biomass for the shallower bank polygons (CB, GB, PE).

The relative distribution of biomass among the three fractions was fairly similar across the polygons (Fig. 3B). The medium fraction made up about 40–60% of the biomass, the small fraction about 25–45%, and the large fraction about 10–20%. The small fraction was on average largest for the Central Bank and Great Bank polygons (CB and GB). The large fraction had lowest contribution (<10%) in the South-West and Svalbard-North polygons (SW and SvN) and tended to be largest in the deep and northern polygons (HD, FVT, NE). The mean values for the polygons are summarized in Table S-16 along with SD and confidence intervals. In absolute values, the large fraction varied between 0.4 (PE) and 1.9 (BIT) g dw m$^{-2}$, the medium fraction between 1.6 (SE) and 5.9 (BIT) g dw m$^{-2}$, and the small fraction between 1.2 (PE) and 3.8 (SN) g dw m$^{-2}$.

The data for the PCA of fractions and total biomass over all polygons and years were labeled in spatial groups of western, central, eastern, and northern polygons (color-coded in Fig. S-2). The results showed considerable spread and overlap between the spatial groups, but with a tendency of central and eastern polygons to be on the side of negative PC1 in the PCA biplot (associated with low biomass), while northern polygons tended to be on the positive side (associated with high biomass).

### 3.5. Temporal changes – Interannual and decadal variations

Time series of variation of total zooplankton biomass for seven polygons from the western and central Barents Sea are shown in Fig. 4A, while the patterns of variation for the mean values (over the seven polygons) for the three size fractions are shown in Fig. 4B. The temporal variation in biomass of the three fractions are shown for two polygons with contrasting patterns (BIT and GB) in Fig. 5, while the results for six more polygons are shown in Supplementary (Fig. S-3).

There were commonalities as well as differences in the temporal patterns among the seven polygons. The biomass tended to be low around 1990, followed by a conspicuous peak in 1994 (Fig. 4A). The
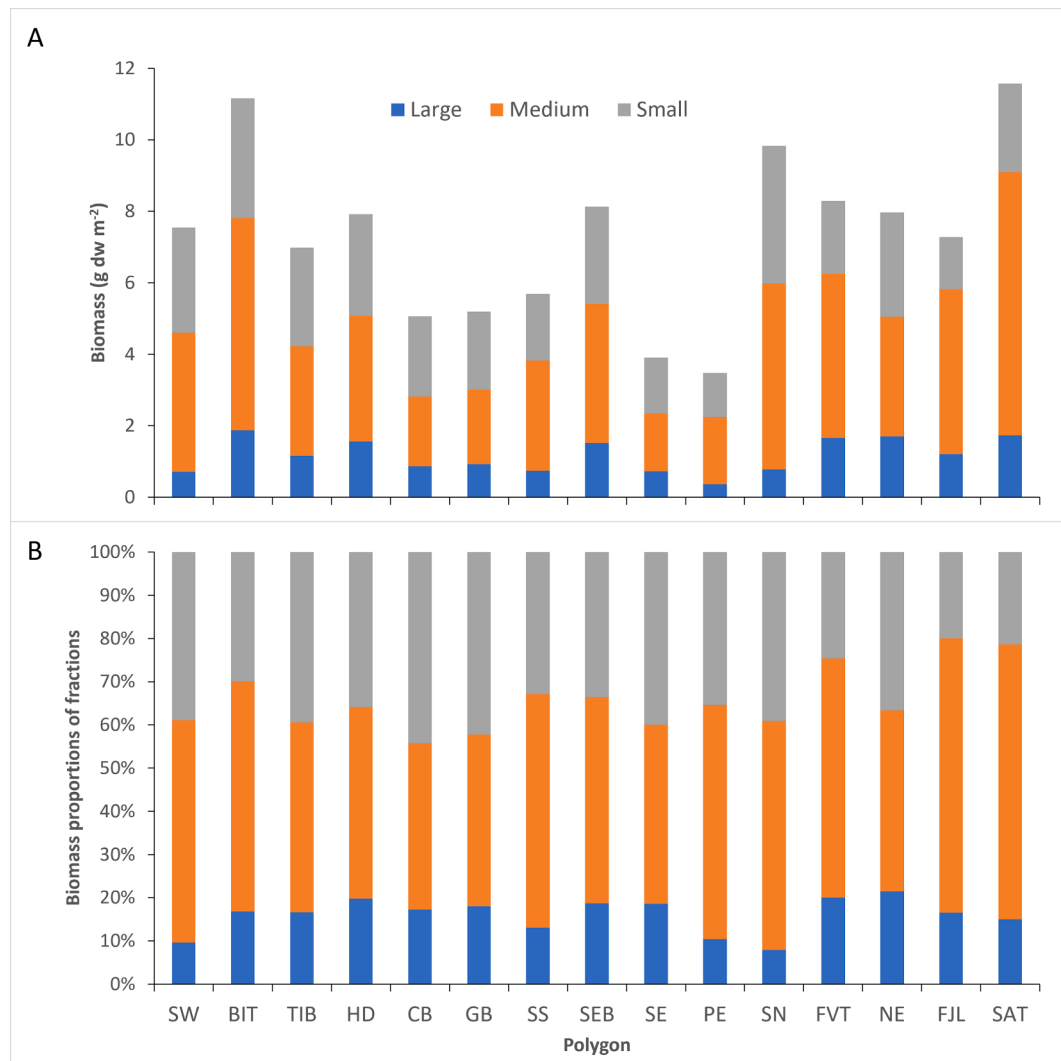
**Fig. 3.** Mean zooplankton biomass in three size fractions (large – >2 mm, medium – 1–2 mm, small – <1 mm) for polygons in the Barents Sea based on data collected 1989–2020. A– cumulative biomass (stacked columns) of the three fractions in units of g dry weight biomass m$^{-2}$. B– Relative (%) contribution of biomass of the three fractions. Annual mean polygon values based on only one or two stations have been excluded from the calculations (see Table S-1 for overview of station numbers).

peak was especially sharp and strong for the three southwestern (Atlantic water) polygons (SW, BIT, HD), with values around 20 g dw m$^{-2}$, and it was driven to considerable extent by the small size fraction but with contribution also from the medium fraction (Fig. 4B and 5A). After the peak, the total biomass declined with a convergence to uniform, moderate biomass of 5–8 g dw m$^{-2}$ in 2003. Since then, there has been a divergence, with general increase for the BIT polygon, decrease for the GB polygon, and more stable (though fluctuating) patterns for other polygons (e.g., HD and TIB) (Figs. 4 and 5).

The total biomass tended to be highest for the BIT polygon (Fig. 4A) and was driven by high contribution of the medium fraction (Fig. 5A). The GB polygon showed generally the lowest total biomass (along with CB; Fig. 4A), and the biomass was often dominated by the small fraction (Fig. 5B). The medium fraction was on average the largest, with no clear temporal trend after about year 2000 for this fraction nor for the small fraction (Fig. 4B). In contrast, the large fraction showed decline to low values in the late part of the time series (Fig. 4B and 5).

The average total biomass for the seven polygons showed a weak declining trend over the time series (r = −0.24), with a slightly better correlation for the last two decades (r = −0.31) driven mainly by decline of the large fraction (Fig. 4B). Statistically significant declining trends in zooplankton biomass over the time series were found for the large

fraction for the BIT, SW, and GB polygons, for the medium fraction for the GB and CB polygons, for the small fraction for the HD polygon, and for total biomass for the GB and HD polygons (Mann-Kendall test, p < 10$^{-2}$-10$^{-4}$; Fig. 6, Fig. S-3). There were no cases of significantly increasing biomass.

### 3.6. Temporal and spatial variation explored by PCA

Principal component analysis (PCA) was run with annual mean values for the seven selected polygons in two versions using total zooplankton biomass and biomass of the three fractions, respectively. Both versions gave broadly similar results. With total biomass, the seven variables (polygons) were aligned with positive PC-1 axis, while they spread out in a spatial pattern along PC-2 with contrast between GB and SW (Fig. S-4A). Using fractions, a similar pattern was seen with all variables (21 combinations of polygons and fractions) aligned with positive PC-1, while they fanned out along PC-2 with a pattern now dominated by a contrast between the large and small fractions (Fig. S-4B).

The patterns from the PCAs demonstrate positive covariation in the temporal patterns in zooplankton biomass of the various polygons, for total biomass as well as biomass of each of the three fractions. This is
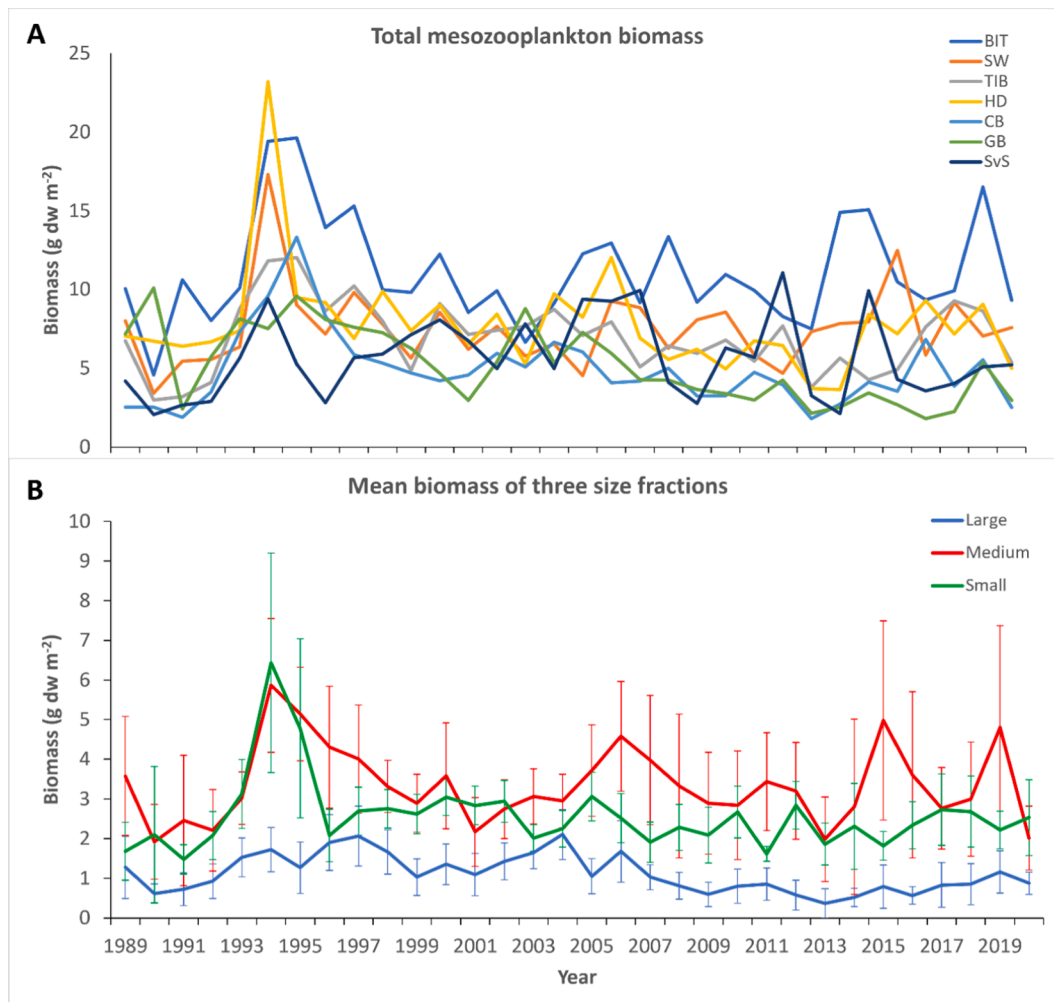
**Fig. 4.** Temporal variation (1989–2020) of (A) total zooplankton biomass in seven polygons from the western and central Barents Sea, and (B) mean biomass of three size fractions for the same seven polygons. See Fig. 1 for location of the polygons. Vertical error lines in B are +/-2*SE based on variation across the annual mean values for the seven polygons (corresponding approximately to +/- 95% confidence interval for single point estimates).

confirmed by positive correlation coefficients (Pearson r) between the polygon series of biomass (Table 4).

The pattern of years in the PCA plots (projections of data points for years onto the PC1-PC2 plane; Fig. S-4) reveal 'outliers', which are 1994 and 1995 with high positive scores on PC1 (high biomass, see Fig. 4), and 1990 (and partly also 1991 and 2013) with high negative scores on PC1 (low biomass). The years 1994 and 1995 are positioned in the lower right quadrant of the PCA plot for fractions (Fig. S-4B), indicating high biomass in the small fraction. 1990 is positioned in the upper left quadrant, indicating low biomass especially for the SW and BIT polygons (Fig. S-4A) and the small fraction (Fig. S-4B).

The time series of PC1 scores, which are coordinates for the data points for years on the PC1 axis, revealed a very similar pattern for the two PCAs for total and fractions, respectively (Fig. 6; r = 0.98). They were also very close to the mean total biomass for the seven polygons (Fig. 6; r = 0.96 (total) and 0.92 (fractions)). This demonstrates that PC1 extracts out the variation in zooplankton biomass with time, and that it represents a time series of zooplankton biomass.

With PC1 being an almost pure axis of variation in zooplankton biomass, PC2 extracts out the maximum residual variance, which represents a spatial pattern with the PCA for total biomass, and a pattern of shift between size fractions with the PCA for biomass of fractions (Fig. S-4). Both PC2's showed a declining trend over the time series, reflecting a qualitative shift in spatial pattern and pattern of fractions (Fig. 7). The two series of PC2 were correlated (r = 0.69), which suggests a

correspondence between change in spatial pattern and shifts among fractions. This probably reflects what is illustrated in Fig. 5, with an increase in biomass driven by the medium fraction in the Atlantic inflow area (BIT), and an opposite trend of decrease in biomass with a relatively large importance of the small fraction for the northern GB polygon.

### 3.7. Relationships with drivers – Capelin stock size and climate

#### 3.7.1. Capelin

We color-coded the years in the PCA plots (Fig. S-4) according to low (<1 million tons) or high (>1 million tons) total stock biomass of the Barents Sea capelin (Fig. 2). There is a relatively clear pattern of 'blue' data points for low capelin stock on the right side of the plots with positive PC1 and high zooplankton biomass, and, vice versa, 'red' data points for high capelin stock on the left side with negative PC1 and low zooplankton biomass.

A non-metric multidimensional scaling analysis of polygon biomass (fractions and total), with capelin stock size and several climate series as explanatory variables, showed basically the same ordination of data points (years) as the PCA (Fig. 8). The time series of scores on axis-1 for the NMDS and PC1 (fractions) were strongly correlated (r = −0.93; note that the axis in Fig. 8 is reversed relative to the PCAs in Fig. S-4). The two measures of capelin stock size (immatures and total) are aligned with axis 1, pointing to the right in direction of low zooplankton biomass (Fig. 8). This reflects a statistically significant inverse relationship
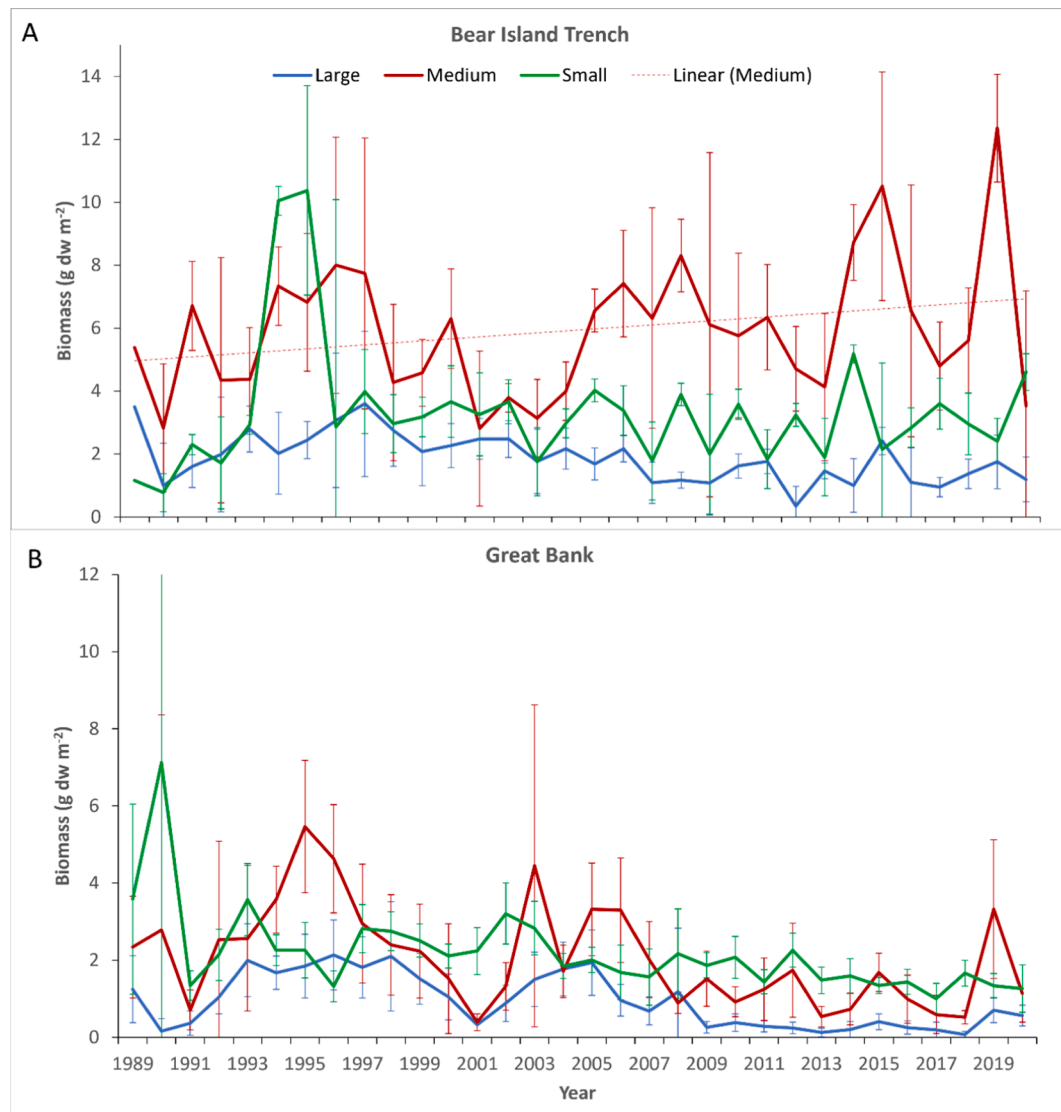
**Fig. 5.** Zooplankton biomass in three size fractions (large – >2 mm, medium – 1–2 mm, and small – <1 mm) from 1989 to 2020 for (A) the Bear Island Trench (BIT), and (B) the Great Bank (GB) polygons. Annual mean values with vertical error bars (+/- 2*SE) for variation among stations in each polygon (see Table S-1 for number of stations).

between zooplankton biomass and size of the capelin stock (r = −0.69 (calculated for linear scale), Fig. 9A). Removing the two high values in 1994 and 1995 (see Discussion) did not change the correlation materially (r = −0.68).

A clear inverse relationship between zooplankton biomass and the capelin stock was seen for the Great Bank (GB) polygon, which is a main feeding area for capelin. Biomass of the large and medium fractions increased and were higher in the periods when the capelin stock was low and decreased to lower values when the capelin stock swung back to high levels (Fig. 10A). This was reflected in negative correlations between capelin and biomass of these two fractions (r = −0.51 and −0.53).

The trend in PC2 for the seven polygons (Fig. 7) suggested a change in patterns among polygons and size fractions. Inspection of plots of time series of the proportions of the three size fractions suggests a divergence among polygons after about year 2005 (Fig. S-5). The two polygons in the inflow region in southwest (SW and BIT) showed high proportion of the medium fraction and low proportion of the small fraction, while the two central polygons (CB and GB) showed the opposite with low proportion of the medium fraction and high proportion of the small fraction (Fig. S-5B, C). The latter polygons constitute the core area for overwintering and summer feeding of capelin (Ingvaldsen and Gjøsæter

2013). The ratio of the small to medium fractions for these two polygons (CB and GB) showed a significant positive correlation with the capelin stock biomass (Fig. 9B), demonstrating a shift to smaller zooplankton with increasing stock size of capelin. The large size fraction showed a decrease for all polygons after 2004, with a less clear difference between the two sets of polygons (inflow region versus capelin core area) (Fig. S-5A).

*3.7.2. Climate*

Climate variables included areas of three water masses (Atlantic, mixed, and Arctic), area of maximum sea ice in winter, temperature and salinity of Atlantic water at the Russian Kola section, and the NAO winter index. The area of water masses, winter sea ice, and Kola temperature are internally correlated (r = 0.51–0.92). These climate indices are arranged in a rotated direction relative to Axis-2, with warm conditions (Kola temperature and areas of Atlantic and mixed waters) on the lower right side, and cold conditions (area of Arctic water and sea ice) on the upper left side (Fig. 8).

The rotated positions of explanatory variables relative to axis 1 and axis 2 in Fig. 8 reveal that there was not a 'clean' separation of the climate variables in explaining variability along the two axes. The
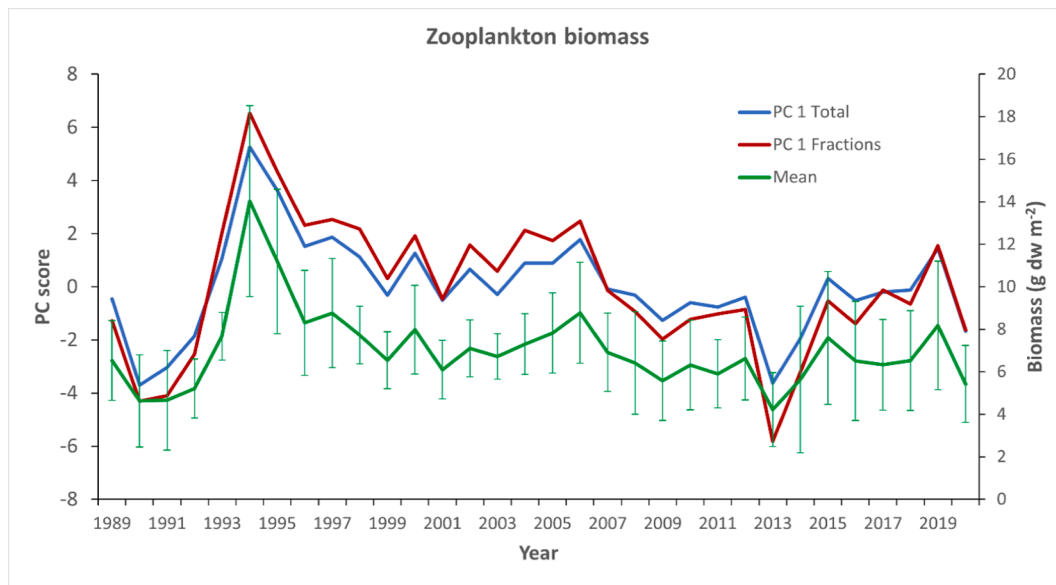
**Fig. 6.** Time series of annual scores on PC1 for two PCAs of total biomass and biomass in three size fractions (large, medium, small), respectively, for seven polygons (BIT, SW, TIB, HD, CB, GB, SvS; see Fig. 1 for location of polygons) in the Barents Sea, 1989–2020. Time series of the arithmetic mean total biomass for the same seven polygons is also shown (y-axis on the right side).

**Table 4**

Pearson r correlation coefficients between time series of zooplankton biomass of seven polygons (BIT, SW, TIB, HD, CB, GB, SvS; see Fig. 1) for total biomass (T) and biomass of three size fractions (L – large, M – medium, and S – small). The r values are given in the lower left part of the matrix, while corresponding p values (probability levels) are given in the upper right part. The p values are not corrected for autocorrelation and multiple comparisons and are used to indicate relative strength of significance only. r values with p < 0.001 and p < 0.01 (for single comparisons) are indicated with bold and italics font, respectively.

| | BIT-T | SW-T | TIB-T | HD-T | CB-T | GB-T | SvS-T |
|---|---|---|---|---|---|---|---|
| BIT-T | | 0.000 | 0.001 | 0.013 | 0.003 | 0.585 | 0.182 |
| SW-T | 0.607b | | 0.010 | 0.029 | 0.218 | 0.680 | 0.223 |
| TIB-T | 0.550i | 0.449 | | 0.002 | 0.000 | 0.050 | 0.022 |
| HD-T | 0.436 | 0.385 | 0.525 | | 0.000 | 0.016 | 0.024 |
| CB-T | 0.509i | 0.224 | 0.767b | 0.657b | | 0.004 | 0.039 |
| GB-T | 0.100 | −0.076 | 0.350 | 0.424 | 0.499i | | 0.239 |
| SvS-T | 0.242 | 0.221 | 0.403 | 0.398 | 0.366 | 0.214 | |

| | BIT-L | SW-L | TIB-L | HD-L | CB-L | GB-L | SvS-L |
|---|---|---|---|---|---|---|---|
| BIT-L | | 0.000 | 0.032 | 0.082 | 0.011 | 0.000 | 0.294 |
| SW-L | 0.657b | | 0.000 | 0.012 | 0.069 | 0.003 | 0.038 |
| TIB-L | 0.380 | 0.584b | | 0.000 | 0.008 | 0.014 | 0.222 |
| HD-L | 0.312 | 0.437 | 0.616b | | 0.000 | 0.017 | 0.011 |
| CB-L | 0.443 | 0.326 | 0.459i | 0.689b | | 0.000 | 0.050 |
| GB-L | 0.625b | 0.514i | 0.429 | 0.418 | 0.647b | | 0.038 |
| SvS-L | 0.191 | 0.368 | 0.222 | 0.445 | 0.350 | 0.368 | |

| | BIT-M | SW-M | TIB-M | HD-M | CB-M | GB-M | SvS-M |
|---|---|---|---|---|---|---|---|
| BIT-M | | 0.000 | 0.058 | 0.170 | 0.025 | 0.332 | 0.089 |
| SW-M | 0.583b | | 0.211 | 0.282 | 0.522 | 0.677 | 0.049 |
| TIB-M | 0.339 | 0.227 | | 0.020 | 0.000 | 0.026 | 0.030 |
| HD-M | 0.249 | 0.196 | 0.410 | | 0.001 | 0.003 | 0.047 |
| CB-M | 0.396 | 0.117 | 0.718b | 0.544i | | 0.005 | 0.045 |
| GB-M | 0.177 | −0.077 | 0.394 | 0.503i | 0.481i | | 0.313 |
| SvS-M | 0.306 | 0.350 | 0.383 | 0.354 | 0.357 | 0.184 | |

| | BIT-S | SW-S | TIB-S | HD-S | CB-S | GB-S | SvS-S |
|---|---|---|---|---|---|---|---|
| BIT-S | | 0.000 | 0.000 | 0.001 | 0.009 | 0.163 | 0.097 |
| SW-S | 0.709b | | 0.000 | 0.029 | 0.220 | 0.177 | 0.261 |
| TIB-S | 0.772b | 0.603b | | 0.003 | 0.000 | 0.671 | 0.164 |
| HD-S | 0.542i | 0.387 | 0.509i | | 0.001 | 0.935 | 0.362 |
| CB-S | 0.451i | 0.223 | 0.714b | 0.563i | | 0.331 | 0.556 |
| GB-S | −0.253 | −0.245 | −0.078 | 0.015 | 0.178 | | 0.586 |
| SvS-S | 0.299 | 0.205 | 0.252 | 0.167 | 0.108 | 0.100 | |

climate variables showed positive relation with axis 1, and negative relation with axis 2, for the 'warm' variables. This was reflected in moderate positive correlations (r ∼ 0.3–0.4) for the climate variables with axis 1, and moderate negative correlations (r ∼ −0.3) with axis 2. Capelin provided the strongest signal (inverse relationship) for the variation in total zooplankton biomass along axis 1 (r = 0.73), while it had low influence on variation along axis 2. Similar correlations (with reversed sign for PC1) were expressed for capelin and climate versus the two PC1s, demonstrating negative correlation between zooplankton biomass and Kola temperature (Table 5). Negative correlation with Kola temperature was also seen for the GB polygon for biomass of the large and medium fractions and total biomass (Fig. 10B, Table 5).

Removing the trends with time in the data series improved the inverse correlations between zooplankton biomass and capelin stock size, most markedly for the total biomass of the GB polygon (Table 5). This demonstrates that the correlations were driven mainly by the inverse oscillations and not by systematic trends in the data over the time series. The opposite was the case for PC-2 (reflecting a shift in spatial pattern and size fractions) with temperature, where removing the trends also removed the correlations. This demonstrates that the correlations reflected the trends (decrease in PC-2 (Fig. 7) and increase in temperature (Fig. 2)) and not fluctuations. For the relations between zooplankton biomass and temperature, removing the trends reduced the negative correlations (most clearly for the GB polygon), although they remained at a level of ∼ −0.3–0.4 (Table 5). This suggests that both the fluctuations and linear trend of the data contributed to the negative correlation (decreasing zooplankton biomass with increasing temperature).

Using PC-1 from the two versions of PCA (total biomass and size fractions) and the mean total biomass of seven polygons as dependent variables in a multivariate multiple linear regression found that capelin stock and Kola temperature had significant effects on the temporal variation of zooplankton biomass (Table 6). Capelin and temperature together explained about 60% of the variance in zooplankton biomass, with capelin as the most important factor contributing about ¾ of the explained variance.

## 4. Discussion

We report results from more than three decades of monitoring of zooplankton biomass in the Barents Sea with a standardized, size-
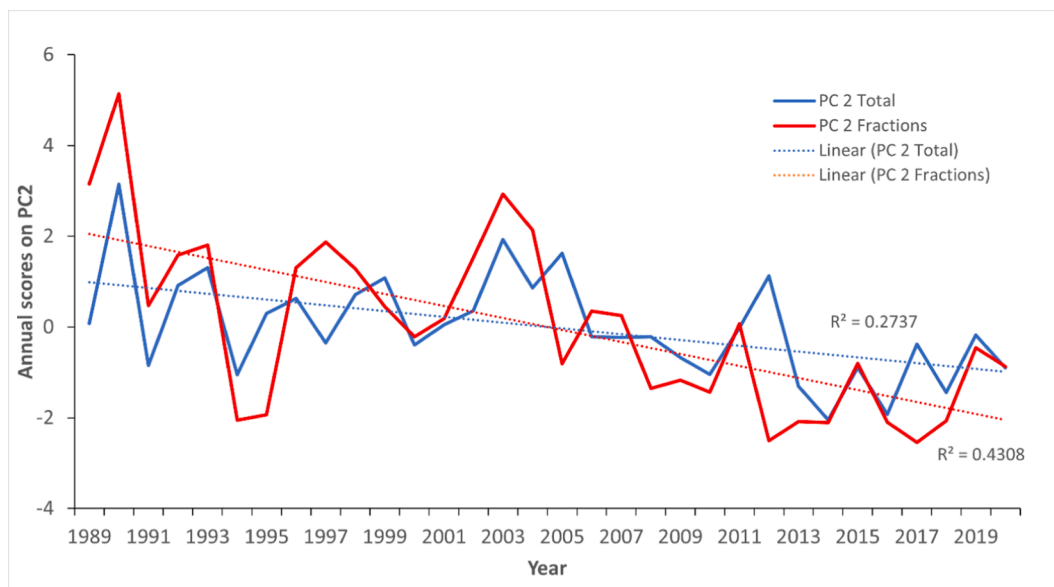
**Fig. 7.** Time series of annual scores on PC2 (coordinates for data points (years) on the second principal component) for the two versions of PCA for total zooplankton biomass and biomass in three size fractions, respectively.
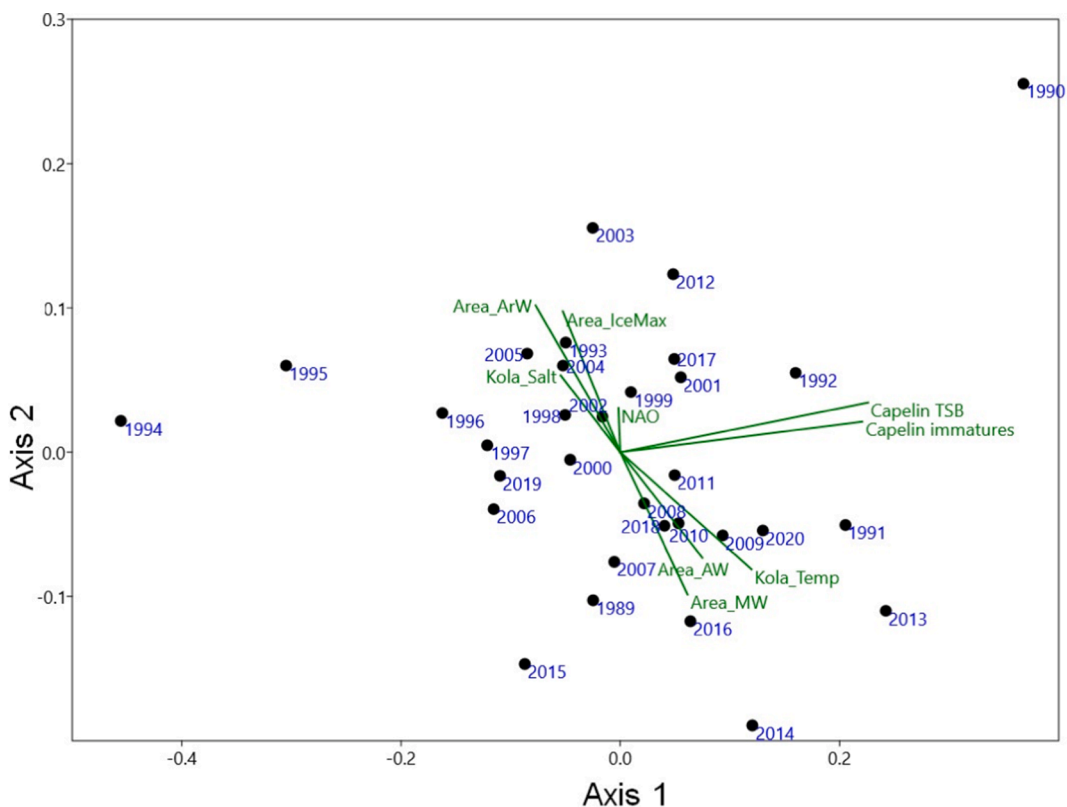


**Fig. 8.** Biplot of axis 1 and axis 2 of a non-metric multidimensional scaling (NMDS) analysis of zooplankton biomass of seven polygons, with projection of years (data points) and explanatory variables (green arrows, identified by labels).

fractionation procedure. The monitoring is done jointly with the Russian partner institute PINRO, as part of coordinated Norway-Russia fisheries investigations (Jakobsen and Ozhigin 2011), which extends the geographical coverage of total zooplankton biomass to include the Russian waters of the eastern Barents Sea (Skjoldal et al., 2018, 2019, Dalpadado et al., 2020). While we report results starting in 1989, data on zooplankton biomass was collected during the decade of the 1980s, mainly from research activities during the spring and summer periods

(Skjoldal et al., 1992, Dalpadado et al., 2003). The decades since the 1980s have seen large changes in the Barents Sea ecosystem, with a pronounced warming of nearly 2 °C and dramatic oscillations of the dominant capelin stock (Fig. 2).

A summary of the main results are: i) a persistent spatial pattern with higher biomass in deeper basins compared to shallower bank areas, ii) a pronounced peak in 1994 driven mainly by the small size fraction, iii) considerable temporal covariation of zooplankton biomass between
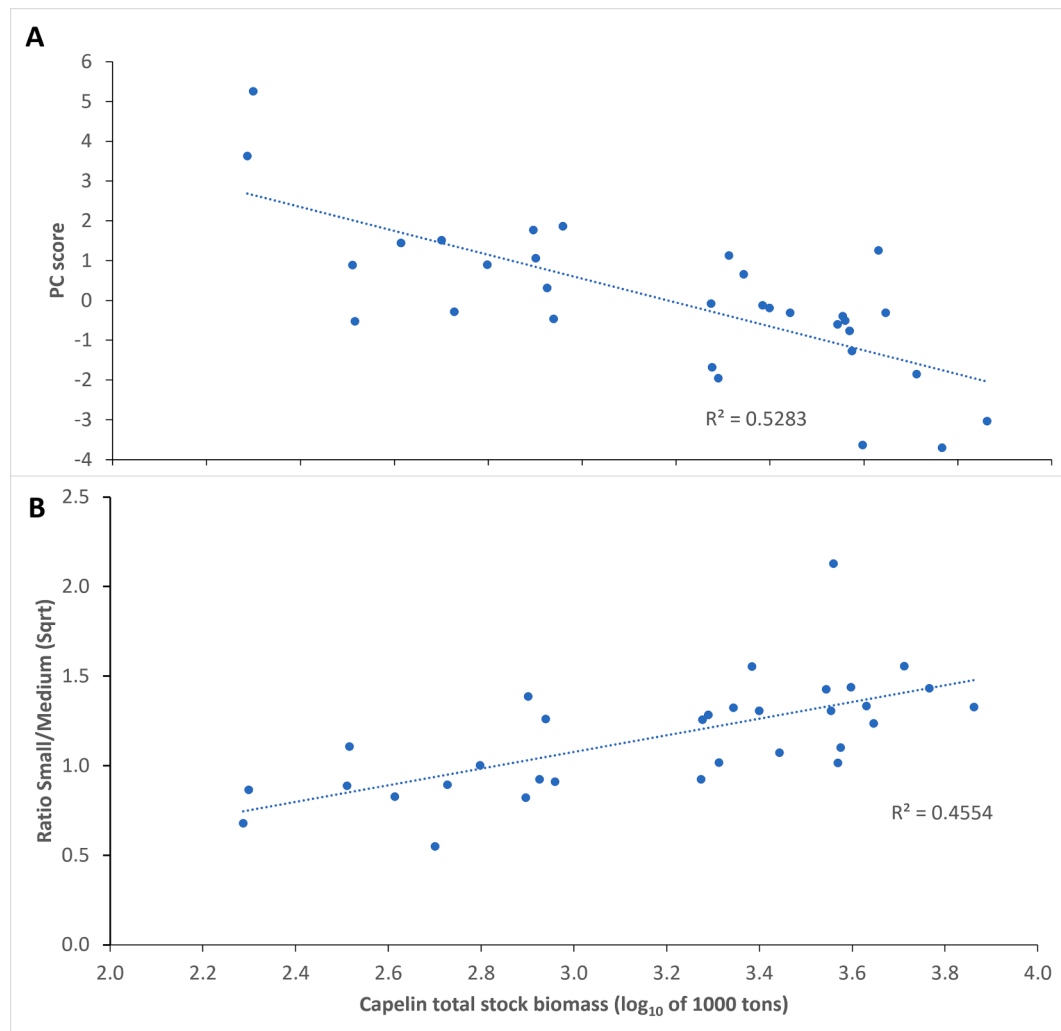
**Fig. 9.** Zooplankton biomass versus capelin stock biomass over the period 1989–2020. A – Average zooplankton biomass for seven polygons (BIT, SW, TIB, HD, CB, GB, SvS) (represented by PC1 from PCA of total biomass; see Fig. 6) plotted against capelin total stock biomass (log10 of units $10^3$ tons). The two high values in the upper left corner are for 1994 and 1995. B – Ratio of biomass of small to medium size fractions (S/M) as average for the CB and GB polygons (which are core areas of capelin) versus capelin biomass (log10). The S/M ratio is square root transformed, and values > 1 show dominance of the small fraction and values < 1 show dominance of the medium fraction. $R^2$ (Pearson r) gives fraction of variance explained by the trend with capelin stock.

different subareas (polygons) of the southern and central Barents Sea, iv) high biomass in the southwestern Atlantic inflow area since about 2005, v) declining trends in biomass for the central area (Central Bank and Great Bank) since the 1990s, vi) a general decline of the large size fraction in the last two decades, vii) inverse relationship between zooplankton biomass and stock size of capelin, and viii) inverse relationship between zooplankton biomass and Atlantic water temperature. In the following, these features of the results are discussed, with emphasis on the roles of the *Calanus* species, advection of Atlantic water into the Barents Sea, and predation impact by capelin.

### 4.1. The variation in biomass is driven by Calanus species

The older copepodite stages of *Calanus finmarchicus* and *C. glacialis*, stage CV and adults, and partly CIV, are contained in the medium size fraction (1–2 mm) (Skjoldal, 2021). These same stages contribute to the build-up of biomass of the *Calanus* species in summer and autumn, with little contribution to biomass by the younger copepodite stages CI-CIII, despite their higher numerical abundance (Aarflot et al., 2018b, Skjoldal et al., 2021). The two *Calanus* species make up most of the meso-zooplankton biomass in the Barents Sea, estimated to be about 80% on average (Aarflot et al., 2018b). This suggests that the medium size

fraction is made up predominantly by *Calanus* and that much of the biomass of *Calanus* is contained in this fraction.

The high correlation (r = 0.9) between the medium fraction and total biomass suggests that variation in the medium fraction, that is variation in biomass of *Calanus* species, drives the overall variation in total biomass in the Barents Sea. This is the same conclusion reached by Aarflot et al. (2018b) and is in line with the dominant roles of the two *Calanus* species in the Barents Sea ecosystem (Tande, 1991, Melle and Skjoldal, 1998, Falk-Petersen et al., 2009). This conclusion is derived from the total material from all polygons reported here and is applicable across the biogeographical transition from the boreal domain in south dominated by *Calanus finmarchicus* to the Arctic domain in north dominated by *C. glacialis*.

### 4.2. Biomass is higher in basins compared to banks

The polygons were drawn up based on topography (and associated differences in hydrography and oceanography), and they differ in including predominantly either basins (e.g., BIT, HD, and SEB) or banks (e.g., CB and GB) (see Fig. 1). The pattern of higher total zooplankton biomass in basin polygons compared to lower biomass in bank polygons may reflect several different mechanisms: i) seasonal descent of
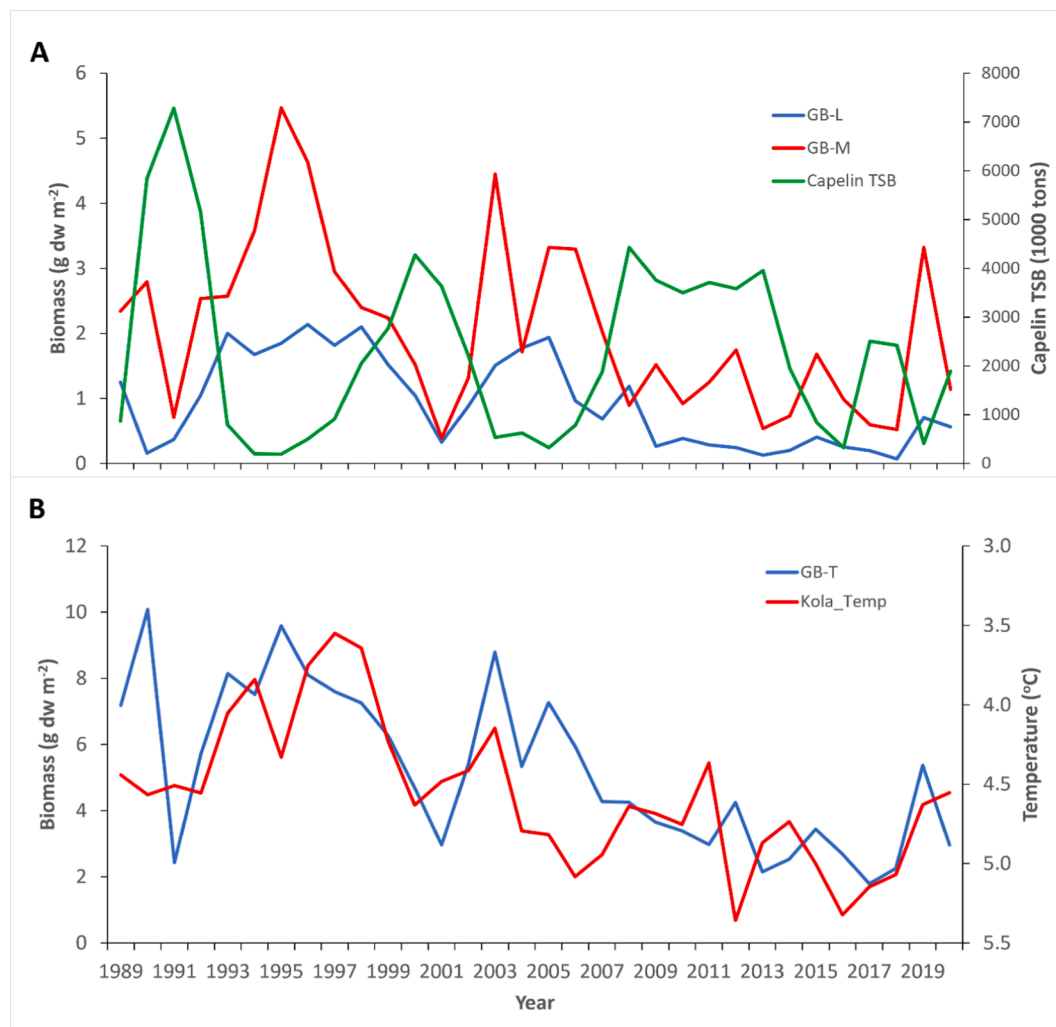
**Fig. 10.** Temporal patterns of (A) zooplankton biomass of the large and medium fractions for the Great Bank (GB) polygon and total stock size of capelin, and (B) total zooplankton biomass for the GB polygon and temperature at the Kola section, 1989–2020. Note the inverted temperature scale.

**Table 5**

Correlation coefficients (Pearson r) between PC1 and PC2 from PCA of zooplankton biomass (total and size fractions), mean total biomass of seven polygons (Mean-T), and biomass of the medium fraction and total (M and T) for the Great Bank (GB) polygon versus capelin stock size (total stock biomass) and temperature at the Kola section. Correlations are calculated for the original data series 1989–2020, and for the data series detrended for time.

|  | Original data | | Detrended data | |
|---|---|---|---|---|
|  | Capelin | Temperature | Capelin | Temperature |
| PC 1 Total | −0.69 | −0.37 | −0.74 | −0.35 |
| PC 1 Fractions | −0.67 | −0.44 | −0.74 | −0.39 |
| Mean-T | −0.64 | −0.38 | −0.70 | −0.31 |
| PC 2 Total | 0.05 | −0.28 | −0.03 | 0.07 |
| PC 2 Fractions | 0.06 | −0.47 | −0.05 | −0.11 |
| GB-M | −0.53 | −0.49 | −0.68 | −0.29 |
| GB-T | −0.35 | −0.61 | −0.64 | −0.31 |

zooplankton into deeper water, ii) higher predation over banks compared to basins, and iii) inclusion of a mesopelagic component of zooplankton in the basins. We note that biomass is depth-integrated over the water column (minus the lower ∼ 10 m), and that volume of water filtered by the zooplankton net is proportional to water depth.

The two *Calanus* species which dominate the zooplankton biomass descend from the surface layer to overwinter at depth. This is particularly well documented for *C. finmarchicus* in the Norwegian Sea where the overwintering stage CV descends into the cold intermediate water layer at 500–1000 m depth (Østvedt, 1955, Melle et al., 2004, 2014). The data we report here are from the autumn period when we expect the *Calanus* species to have completed the seasonal development based on phytoplankton in the upper layer and to have migrated deeper in the water column. The downward migration combined with water currents may flush *Calanus* individuals off the banks and concentrate them in deeper areas. For *Calanus glacialis*, individuals may be transported off Arctic banks with the flow of denser water formed over the banks in winter and draining off the banks during the following summer (Aarthun et al., 2012).

Higher mortality from visual predators (such as capelin and other planktivorous fishes) over shallower banks compared to deeper waters is a potential mechanism causing lower biomass over banks (Aarflot et al., 2018a). Shallower topography may block the descent of zooplankton, keeping them in a zone of sufficient light for detection by visual predators such as capelin. The effect of this topographic blockage mechanism would depend on the specific circumstances of the configuration and depth of a bank and the associated water circulation. The strength of the effect of topographic blockage is expected to be less over deep banks such as the Central and Great banks where water depth of 150–200 m may provide sufficiently low light levels to effectively reduce the predation impact by visual predators in the deeper part of the water column.

*Calanus finmarchicus* is a predominant herbivore that grows and

**Table 6**

Results of multivariate multiple linear regression of zooplankton biomass (PC-1 total and fractions, mean total biomass for seven polygons) as dependent variables versus capelin stock size and Kola temperature as independent variables for the data series 1989–2020.

| Tests on dependent variables | | | | | |
| --- | --- | --- | --- | --- | --- |
| | $R^2$ | F | df1 | df2 | p |
| PC 1 Total | 0.548 | 17.58 | 2 | 29 | 1.00E-05 |
| PC 1 Fractions | 0.568 | 19.04 | 2 | 29 | 5.25E-06 |
| Mean-T | 0.490 | 13.91 | 2 | 29 | 5.80E-05 |

| Regression coefficients and statistics | | | | | | |
| --- | --- | --- | --- | --- | --- | --- |
| | | Coeff. | Std.err. | t | p | $R^2$ |
| PC 1 Total | Constant | 6.46 | 2.34 | 2.76 | 0.0098 | |
| | Capelin TSB | −0.00065 | 0.00013 | −5.13 | 1.79E-05 | 0.479 |
| | Kola_Temp | −1.086 | 0.517 | −2.10 | 0.044 | 0.138 |
| PC 1 Fractions | Constant | 10.73 | 3.16 | 3.39 | 0.002 | |
| | Capelin TSB | −0.00086 | 0.00017 | −5.01 | 2.50E-05 | 0.456 |
| | Kola_Temp | −1.91 | 0.698 | −2.74 | 0.010 | 0.194 |
| Mean-T | Constant | 13.93 | 2.53 | 5.50 | 6.34E-06 | |
| | Capelin TSB | −0.00061 | 0.00014 | −4.40 | 0.0001 | 0.409 |
| | Kola_Temp | −1.20 | 0.560 | −2.15 | 0.040 | 0.149 |

develops by grazing on phytoplankton in the upper water layer where it is part of the epipelagic zooplankton community during spring and summer. When it descends to overwinter in deep water, it becomes part of the mesopelagic community. In the adjacent and deep Norwegian Sea, there is a rich mesopelagic community also in summer with biomass for the 200–700 m depth layer found to be about 50% compared to the biomass in the upper 200 m (Melle et al., 2004). The inflow region to the Barents Sea in the Bear Island Trench has a maximum depth of about 500 m, and the upper part of the mesopelagic layer is available for advective transport into the deeper portions of the Barents Sea shelf. The mesopelagic component is possibly a main reason for the consistently highest biomass in the BIT polygon (Fig. 3A).

### 4.3. Effects of warming and 'borealization' – Increase of Calanus finmarchicus and decrease of C. glacialis

Much of the Barents Sea shelf is a biogeographical transition zone between the boreal Atlantic and the Arctic biogeographical and bioclimatic zones. With the recent and ongoing warming, the boreal Atlantic zone has been expanding and the Arctic zone has been declining in what has been termed 'Atlantification' and 'borealization' (Fossheim et al., 2015, Ingvaldsen et al., 2021). Modelling results have indicated an expansion of *Calanus finmarchicus* and a reduction of *C. glacialis* in response to the warming (Slagstad et al., 2011, Skaret et al., 2014, Dalpadado et al., 2012, 2020).

We interpret the increased zooplankton biomass dominated by the medium size fraction in the BIT polygon from around 2005 (Fig. 5A) as due to an increased amount of *Calanus finmarchicus*. Monitoring of *C. finmarchicus* on the Fugløya-Bear Island transect across the Barents Sea opening since 1995 has shown an increased abundance of older copepodite stages in summer (June and August), which was interpreted to reflect increased abundance of a second generation under the recent warmer ocean climate (Skjoldal et al., 2021). Aarflot et al. (2018b) reported similar increases in zooplankton biomass and proportion of *C. finmarchicus* in the western inflow region of the Barents Sea. A second generation of *C. finmarchicus* in the southwestern Barents Sea in late summer was indicated in a model study (Skaret et al., 2014) and was reported from data analyses by Gluchowska et al. (2017) and Strand et al. (2020) for Atlantic water in the northeastern Norwegian Sea and the entrance region to the Barents Sea.

The decrease in zooplankton biomass for the CB and GB polygons (Fig. 5B) is interpreted to reflect a decline in *Calanus glacialis*. The Central Bank used to be in the Arctic domain with sea ice formation and ice cover in winter (Quadfasel et al., 1992). *C. glacialis* was the dominant species in the Arctic water mass, while it occurred in mixed assemblage

with *C. finmarchicus* in the Polar Front region with vertical layering and mixing of Arctic and Atlantic waters (Hassel, 1986, Melle and Skjoldal, 1998, Hirche and Kosobokova, 2003). The strong decline in zooplankton biomass by a factor of two or more from the 1990s to the 2010s for the CB and GB polygons is interpreted to reflect a pronounced decrease in abundance of *C. glacialis* in these central areas of the Barents Sea. The decline was most marked for the medium ('*Calanus*') fraction, with a shift to dominance of the small size fraction (Fig. 5B).

The decline of *Calanus glacialis* was likely driven by a combination of climate warming and predation impact by the capelin stock, which is discussed in the following section. The climate warming is itself a complex phenomenon which affects sea ice and hydrography, and likely also water circulation associated with the banks. The CB polygon has become mostly ice-free after 2005, while the GB polygon has had a marked reduction in sea ice (Dalpadado et al., 2020). This has been associated with an earlier start of the spring phytoplankton bloom and a substantial increase in seasonally integrated primary production based on satellite remote sensing data (Dalpadado et al., 2020). The temperature of the subsurface water layer (30–100 m) at the Central Bank increased by nearly 2 °C (from about 2 to 4 °C) since the late 1980s, while the temperature at the Great Bank increased from sub-zero to positive temperature after 2005 (Fig. S-6; Skagseth, 2018).

The changes in sea ice and hydrography have likely affected the phenology of *Calanus glacialis*, which has been shown to spawn associated with the early increase of chlorophyll *a* in spring (Melle and Skjoldal, 1998). *C. glacialis* has mainly a two-year life cycle in the Arctic water of the northern Barents Sea (Tande, 1991, Melle and Skjoldal, 1998), and warming combined with earlier and stronger growth of phytoplankton may have affected the generational development. In addition, reduced ice formation in winter affects the local production of Arctic water, which again may have influenced the circulation and resupply of *C. glacialis* from core areas in the northern Barents Sea. The details of how warming and the associated loss of sea ice and increased primary production have affected *C. glacialis* in the central Barents Sea remain to be investigated, and the preserved and stored samples for taxonomic analysis (for every biomass sample) may allow documentation of the temporal sequence of change.

### 4.4. Top-down effects from capelin grazing

The strongest trend in the zooplankton biomass data was an inverse relationship with the stock size of capelin (Figs. 8 and 9A). This was seen for both the total data set for seven polygons as well as for selected polygons in the core capelin feeding area in summer, notably the GB polygon. The inverse relationship suggests a strong top-down impact

from capelin predation on zooplankton biomass in the Barents Sea. This confirms previous studies based on partly the same data sources used in the present study (Gjøsæter et al., 2002, Dalpadado et al., 2002, 2003, 2020, Johannesen et al., 2012, Stige et al., 2014). The early studies were based on the strong fluctuations of the capelin stock in the 1980s and 1990s (Gjøsæter et al., 2002, Dalpadado et al., 2002, 2003). Johannesen et al. (2012) found inverse relationship between zooplankton biomass and capelin stock size for the 1984–2009 period, with stronger (negative) correlations during the 1980s and 90s than in the 2000s.

Stige et al. (2014) used data for the same period (extended to 2010), with size fractioned biomass from 1986, to explore statistical relationships with various climatic variables and stock size of capelin and other planktivorous fishes. They found clear inverse patterns of fluctuations between the capelin stock and zooplankton biomass of the medium and large fractions for the central and northern Barents Sea. The inverse relationship was less clear for the southwestern region located largely 'upstream' of the capelin stock. Dalpadado et al. (2020) used the same data of total biomass for polygons (1989–2017) as used here, but including Russian data for the eastern Barents Sea. They reported a similar inverse correlation (r = −0.66) between the capelin stock and total zooplankton biomass for the whole Barents Sea as we report here for the seven western and central polygons (r = −0.64–0.69, Table 5). Dalpadado et al. (2020) also reported significant negative correlations between the capelin stock and zooplankton biomass for the CB, GB and TIB polygons as well as for the BIT and SW polygons.

The pronounced peak in biomass in 1994 in the Atlantic water region in the southwestern Barents Sea (BIT, SW, and HD; Fig. 4A) coincided with a collapse of the capelin stock to low values (Fig. 2). The biomass peak occurred in the inflowing Atlantic water, 'upstream' of the core area of grazing by capelin. It is therefore unlikely that the peak was a response to lower predation impact from capelin but instead was an advective signal from the upstream Norwegian Sea (see next section). Dalpadado et al. (2020) removed the first part of the time series (1989–1996) and recalculated correlations for the shorter series 1997–2017. Correlations were still negative (inverse relationship) but lower and not statistically significant. In our case, when we removed the two peak years 1994 and 1995, the negative correlation was slightly lower (r = −0.61 versus −0.73) but still statistically significant.

### 4.5. Role of advection from the Norwegian Sea

Advection (transport) of water from the adjacent Norwegian Sea by the two main currents (the Norwegian Atlantic Current and Norwegian Coastal Current) plays a fundamental role for the functioning of the Barents Sea ecosystem, which is to large extent a flow-through system. Continued supply of *Calanus finmarchicus* with the inflowing water is required to maintain the population in the southern Barents Sea, which otherwise would be flushed out with the northbound water (Skaret et al., 2014, Kvile et al., 2017). As we have discussed, advection of warmer Atlantic water has probably led to an increase in a second (summer) generation of *C. finmarchicus* in the southwestern inflow region, contributing to the ongoing 'borealization' (Ingvaldsen et al., 2021).

The large fraction showed a marked decrease for all polygons after 2004 (Fig. 5, Fig. S-5A). While predation from capelin is a likely cause for the decline in the core capelin area (e.g., GB, Fig. 10A), the decline in the inflow region (SW and BIT polygons) was likely reflecting lower biomass of the large fraction in the waters from the Norwegian Sea. A possible reason for the reduced biomass of large plankton is the increase and northward expansion in the Norwegian Sea of the large Northeast Atlantic mackerel stock which took place at this time from around 2005 (Jansen et al., 2016, Nøttestad et al., 2016).

### 4.6. Combined effect of climate and capelin predation

Climate is a broad term that includes all aspects of the physical environment, notably the dynamics of ocean currents, properties of

water masses such as temperature and salinity, and vertical stratification, which affects the seasonal development of phytoplankton. Sea water temperature, as one climate parameter, has a complex spatial–temporal expression, and it will affect in principle all organisms through the general effect of temperature on life processes. Ocean temperature is in turn related to the other aspects of climate such as currents and stratification. We have used the temperature of Atlantic water at the Kola transect as a climate index, recognizing that it can be representative for direct and indirect effects of temperature on zooplankton, as well as a proxy for other aspects of the climate. We note that in our case, the NAO index, which is related to strength of currents, had low explanatory effect on the zooplankton biomass variations (Fig. 8).

The Kola temperature was inversely related to zooplankton biomass (see Fig. 8 and Table 5). The inverse correlation was reflecting mainly the temperature fluctuations (Fig. 2) since removing trends with time (years) did not materially change the negative correlations. The Kola temperature was also negatively correlated with PC2 (which can be seen from Fig. 8). In this case, however, the correlation reflected the linear trends since it disappeared after detrending the data (Table 5). PC2 reflected a change in patterns among polygons and size fractions. The change took place as a trend over time (Fig. 7) related to the trend of general warming (Fig. 2). We interpret the change as reflecting the two opposing patterns of an increase in biomass in the inflow region (due to a second generation of *Calanus finmarchicus*) and a decrease of biomass in the central area (due to a decline in *C. glacialis*). The first pattern is likely reflecting a direct effect of temperature on the generational development of *C. finmarchicus* (Skjoldal et al., 2021).

The second feature of decline in biomass in the central area is likely a combined effect of capelin predation and climate. There are several factors and mechanisms that could have contributed to the decline. The disappearance and reduced extent of sea ice would allow capelin to start to feed earlier in spring due to improved light conditions for visual predation of zooplankton prey (Langbehn and Varpe, 2017, Aarflot et al., 2018b, Dalpadado et al., 2020). There may also have been a direct physical effect on the spatial–temporal dynamics of *Calanus glacialis* related to accelerated generational development and altered replenishment of the local occurrence of *C. glacialis* from the wider population in north.

Our data suggest a clear top-down effect of capelin predation affecting both the total biomass and size composition of zooplankton (Fig. 9). Capelin is the largest component among planktivorous fishes in the Barents Sea (Eriksen et al., 2017), and with its large stock size it has the potential to markedly affect the concentration field of its zooplankton prey. This is particularly the case for larger prey which are selected by capelin (Dalpadado and Skjoldal, 1996, Orlova et al., 2010). Predation as the cause for the inverse relationship between capelin and zooplankton biomass is therefore a plausible mechanism. However, there appears also to be an element of coincidence for the inverse relationship since a negative correlation between capelin and zooplankton also exists for the inflow region (BIT and SW polygons) which are positioned 'upstream' of the capelin stock (Dalpadado et al., 2020). The covariation in the temporal patterns for different polygons (Table 4) suggests a large-scale climate influence on zooplankton which may propagate with the currents inside the Barents Sea. The strong peak of zooplankton biomass in 1994 (and partly 1995) in the inflow region (Fig. 4A) is a noticeable feature in this context. It occurred as a peak when the capelin stock had collapsed, apparently without being caused by low capelin predation, and it had a marked influence on the inverse relation between capelin and zooplankton biomass, particularly for shorter time series.

## 5. Conclusions

Results on size-fractioned zooplankton biomass (depth-integrated as dry weight biomass m$^{-2}$) from large-scale monitoring of the Barents Sea

over >3 decades (1989–2020) showed a persistent spatial pattern overlaid by some differences in temporal decadal patterns. The spatial pattern showed generally higher biomass over deeper basin areas compared to shallower bank areas. This could reflect a combination of three factors: seasonal descent of zooplankton such as the mostly herbivorous *Calanus* species into deeper areas, stronger predation impact over banks, and inclusion of a layer of mesopelagic zooplankton in the basins.

The temporal pattern (interannual and decadal) showed a pronounced peak in 1994 and 1995, driven to a considerable extent by the small size fraction. This was a major 'high biomass' event in the Barents Sea, unique over the more than three decades of observations. The event occurred in the inflow region of Atlantic water in the southwestern Barents Sea and was probably a phenomenon advected from the adjacent Norwegian Sea. The dominance of the small fraction suggests that it was not reflecting an increase in *Calanus finmarchicus* (at least not primarily), but what species drove this conspicuous peak in biomass remains to be investigated.

Zooplankton biomass in different subareas (polygons) of the western and central Barents Sea showed some degree of synchronous interannual variation. This suggests a large-scale effect, probably by some aspect of climate which acts to give similar fluctuations in different geographical areas. Zooplankton biomass overall (as an average of seven polygons) showed an inverse relationship with temperature of the Atlantic water at the Kola section, which furthermore suggests an influence of climate.

Zooplankton biomass fluctuated inversely with biomass of the capelin stock, which is taken to reflect top-down predation impact. The inverse pattern was most clearly seen in the central area (Central Bank and Great Bank) which is part of the core feeding area of capelin. However, an inverse pattern (statistically significant) was also found between capelin and zooplankton biomass in the inflow region of Atlantic water located 'upstream' of the capelin stock. This correlation is likely coincidental and reflects probably a climate signal which interacts with and confounds the predation effect by capelin. We conclude that the inverse relation between zooplankton biomass and capelin is a combined effect of predation and climate, with predation being apparently the strongest in the capelin feeding area.

The zooplankton biomass showed different patterns between the southwestern inflow region and the central part of the Barents Sea after about 2005, related to an effect of warming on the phenology of the two dominant *Calanus* species through accelerated development. The biomass increased to relatively high level in the inflow region, interpreted to reflect an increase due to a second summer generation of the boreal *C. finmarchicus*. In contrast, the biomass in the central area showed a decline due to reduction in abundance of the Arctic *C. glacialis*. The changes in the two *Calanus* species are effects of 'borealization' and are likely associated with major influences on the Barents Sea ecosystem. A second generation of *C. finmarchicus* may represent improved feeding conditions for juvenile herring and pelagic young-of-year (0-group) boreal fishes such as cod and haddock in the southern Barents Sea. The consequences of the decline of *C. glacialis* are more difficult to predict. One aspect is the potential shift from a 2-year to a one-year life cycle, which may increase the productivity of this species. Another aspect is the potential expansion of *C. finmarchicus* into previous territory of *C. glacialis*, as well as northward expansion of boreal macrozooplankton such as the krill species *Thysanoessa inermis*.

The decline in zooplankton biomass associated with high capelin stock size was related to a shift to more dominance of the small size fraction. This probably reflected a shift from *Calanus* species to small copepods (such as *Pseudocalanus*) and others. The trends of decline in zooplankton and shift to smaller forms in the recent decade reflected an assumed decrease in the dominant Arctic species *Calanus glacialis*. Less or no sea ice have allowed capelin to start feeding earlier in spring or summer, thus increasing the predation impact on *C. glacialis* which may have a two-year life cycle. This represents a combined physical (climate) and biological effect on zooplankton. In addition, altered physical

conditions (e.g., circulation) related to loss of sea ice may have negatively impacted the replenishment of *C. glacialis* from its core distribution area in the northern Barents Sea. The change to smaller forms of zooplankton is likely to have lowered the transfer efficiency from phytoplankton to higher trophic levels mediated through the zooplankton component of the ecosystem.

### Author contributions

HRS prepared data and wrote the manuscript. EE performed statistical analyses. All co-authors contributed to and reviewed the manuscript.

### Declaration of Competing Interest

The authors declare that they have no known competing financial interests or personal relationships that could have appeared to influence the work reported in this paper.

### Appendix A. Supplementary material

Supplementary data to this article can be found online at https://doi.org/10.1016/j.pocean.2022.102852.

### References

Aarflot, J.M., Aksnes, D.L., Opdal, A.F., Skjoldal, H.R., Fiksen, Ø., 2018a. Caught in broad daylight: Topographic constraints of zooplankton depth distributions. Limnol. Oceanogr. 64 (3), 1–11.

Aarflot, J.M., Skjoldal, H.R., Dalpadado, P., Skern-Mauritzen, M., Fields, D., 2018b. Contribution of *Calanus* species to the mesozooplankton biomass in the Barents Sea. ICES J. Mar. Sci. 75 (7), 2342–2354.

Ådlandsvik, B., Loeng, H., 1991. A study of the climatic system in the Barents Sea. Polar Res. 10 (1), 45–50.

AFWG, 2021. Arctic Fisheries Working Group (AFWG). ICES Scientific Reports. 3 (58).

Årthun, M., Eldevik, T., Smedsrud, L.H., Skagseth, Ø., Ingvaldsen, R.B., 2012. Quantifying the influence of Atlantic heat on Barents Sea ice variability and retreat. J. Clim. 25, 4736–4743.

Conover, R.J., 1988. Comparative life histories in the genera *Calanus* and *Neocalanus* in high latitudes of the northern hemisphere. Hydrobiologia 167 (168), 127–142.

Daase, M., Falk-Petersen, S., Varpe, Ø., Darnis, G., Søreide, J.E., Wold, A., Leu, E., Berge, J., Philippe, B., Fortier, L., 2013. Timing of reproductive events in the marine copepod *Calanus glacialis*: a pan-Arctic perspective. Can. J. Fish. Aquat. Sci. 70 (6), 871–884. https://doi.org/10.1139/cjfas-2012-0401.

Dalpadado, P., Skjoldal, H.R., 1996. Abundance, maturity and growth of the krill species *Thysanoessa inermis* and *T. longicaudata* in the Barents Sea. Mar. Ecol. Prog. Ser. 144, 175–183.

Dalpadado, P., Bogstad, B., Gjøsæter, H., Mehl, S., and Skjoldal, H.R., 2002. Zooplankton–fish interactions in the Barents Sea. In Large Marine Ecosystems of the North Atlantic, pp. 269–291. Ed. by K. Sherman and H. R. Skjoldal. Elsevier Science, Amsterdam.

Dalpadado, P., Ingvaldsen, R., Hassel, A., 2003. Zooplankton biomass variation in relation to climatic conditions in the Barents Sea. Polar Biol. 26 (4), 233–241.

Dalpadado, P., Ingvaldsen, R.B., Stige, L.C., Bogstad, B., Knutsen, T., Ottersen, G., Ellertsen, B., 2012. Climate effects on Barents Sea ecosystem dynamics. ICES J. Mar. Sci. 69 (7), 1303–1316. https://doi.org/10.1093/icesjms/fss063.

Dalpadado, P., Arrigo, K.R., Hjøllo, S.S., Rey, F., Ingvaldsen, R.B., Sperfeld, E., van Dijken, G.L., Stige, L.C., Olsen, A., Ottersen, G., 2014. Productivity in the Barents Sea - response to recent climate variability. PLoS ONE 9 (5). https://doi.org/10.1371/journal.pone.0095273.

Dalpadado, P., Arrigo, K.R., van Dijken, G.L., Skjoldal, H.R., Bagøien, E., Dolgov, A.V., Prokopchuk, I.P., Sperfeld, E., 2020. Climate effects on temporal and spatial dynamics of phytoplankton and zooplankton in the Barents Sea. Prog. Oceanogr. 185, 102320.

Degtereva, A.A., 1979. Regularities of quantitative development of zooplankton in the Barents Sea. Trudy PINRO, Murmansk 43, 22–53 (in Russian).

Dippner, J.W., Ottersen, G., 2001. Cod and climate variability in the Barents Sea. Climate Research 17 (1), 73–82.

Drinkwater, K.F., Harada, N., Nishino, S., Chierici, M., Danielson, S.L., Ingvaldsen, R.B., Kristiansen, T., Hunt, G.L., Mueter, F., Stiansen, J.E., Anderson, S., 2021. Possible future scenarios for two major Arctic Gateways connecting Subarctic and Arctic marine systems: I. Climate and physical–chemical oceanography. ICES J. Mar. Sci. 78 (9), 3046–3065.

Edvardsen, A., Petersen, J.M., Slagstad, D., Semenova, T., Timonin, A., 2006. Distribution of overwintering *Calanus* in the North Norwegian Sea. Ocean Sci. 2, 87–96.

Eldevik, T., Smedsrud, L.H., Li, C., Årthun, M., Madonna, E., Svendsen, L., 2021. The Arctic Mediterranean. In: Mechoso, C.R. (Ed.), Interacting Climates of Ocean Basins. Cambridge University Press, pp. 186–215. 978-1-108-49270-6.

Eriksen, E., Bogstad, B., Nakken, O., 2011. Ecological significance of 0-group fish in the Barents Sea ecosystem. Polar Biol. 34, 647–657. https://doi.org/10.1007/s00300-010-0920-y.

Eriksen, E., Skjoldal, H.R., Gjøsæter, H., Primicerio, R., 2017. Spatial and temporal changes in the Barents Sea pelagic compartment during the recent warming. Prog. Oceanogr. 151, 206–226. https://doi.org/10.1016/j.pocean.2016.12.009.

Eriksen, E., Gjøsæter, H., Prozorkevich, D., Shamray, E., Dolgov, A., Skern-Mauritzen, M., Stiansen, J.E., Kovalev, Yu., Sunnanå, K., 2018. From single species surveys towards monitoring of the Barents Sea ecosystem. Prog. Oceanogr. 166, 4–14.

Eriksen, E., Benzik, A.N., Dolgov, A.V., Skjoldal, H.R., Vihtakari, M., Johannesen, E., Prokhorova, T.A., Keulder-Stenevik, F., Prokopchuk, I., Strand, E., 2020. Diet and trophic structure of fishes in the Barents Sea: the Norwegian-Russian program "Year of stomachs" 2015–establishing a baseline. Prog. Oceanogr. 183, 102262.

Falk-Petersen, S., Mayzaud, P., Kattner, G., Sargent, J.R., 2009. Lipids and life strategy of Arctic *Calanus*. Mar. Biol. Res. 5 (1), 18–39.

Fossheim, M., Primicerio, R., Johannesen, E., Ingvaldsen, R.B., Aschan, M.M., Dolgov, A. V., 2015. Recent warming leads to a rapid borealization of fish communities in the Arctic. Nat. Clim. Change 5 (7), 673–677.

Giske, J., Skjoldal, H.R., Slagstad, D., 1998. Ecological modelling for fisheries. In: Rødseth, T. (Ed.), Models for multispecies management. Physical Verlag, Heidelberg, pp. 11–68.

Gjøsæter, H., Dalpadado, P., Hassel, A., 2002. Growth of Barents Sea capelin (*Mallotus villosus*) in relation to zooplankton abundance. ICES J. Mar. Sci. 59, 959–967.

Gjøsæter, H., Bogstad, B., Tjelmeland, S., 2009. Ecosystem effects of three capelin stock collapses in the Barents Sea. Mar. Biol. Res. 5, 40–53.

Gluchowska, M., Dalpadado, P., Beszczynska-Möller, A., Olszewska, A., Ingvaldsen, R.B., Kwasniewski, S., 2017. Interannual zooplankton variability in the main pathways of the Atlantic water flow into the Arctic Ocean (Fram Strait and Barents Sea branches). ICES J. Mar. Sci. 74 (7), 1921–1936.

Hammer, O., Harper, D.A.T., Ryan, P.D., 2001. PAST: Paleontological statistics software package for education and data analysis. Palaeontol. Electronica 4 (1), 9.

Hassel, A., 1986. Seasonal changes in zooplankton composition in the Barents Sea, with special attention to *Calanus* spp. (Copepoda). J. Plankton Res. 8 (2), 329–339.

Hassel, A., Skjoldal, H.R., Gjøsæter, H., Loeng, H., Omli, L., 1991. In: Sakshaug, E., Hopkins, C.C.E., Øritsland, N.A. (Eds.), Impact of grazing from capelin (*Mallotus villosus*) on zooplankton: A case study in the northern Barents Sea in August 1985 10 (2), 371–388.

Hassel, A., Endresen, B., Martinussen, M.B., Gjertsen, K., Knutsen, T. and Johannessen, M. E., 2020. Håndbok for forskningsgruppe Plankton. Prøvetaking og analyse. Prosedyrer for prøvetaking og pre-analyse av dyre- og planteplankton på forskningsfartøy og i laboratorium på land, Version 6.0, Institute of Marine Research, Bergen, Norway, p. 173 (in Norwegian).

Helaouët, P., Beaugrand, G., 2007. Macroecology of *Calanus finmarchicus* and *C. helgolandicus* in the North Atlantic Ocean and adjacent seas. Mar. Ecol. Prog. Ser. 345, 147–165.

Helaouët, P., Beaugrand, G., Reid, P.C., 2011. Macrophysiology of *Calanus finmarchicus* in the North Atlantic Ocean. Prog. Oceanogr. 91 (3), 217–228.

Hirche, H.-J., Kosobokova, K., 2003. Early reproduction and development of dominant calanoid copepods in the sea ice zone of the Barents Sea – need for a change of paradigms? Mar. Biol. 143 (4), 769–781.

Hirche, H.J., Kosobokova, K.N., 2007. Distribution of *Calanus finmarchicus* in the northern North Atlantic and Arctic Ocean – expatriation and potential colonization. Deep-Sea Research Part II 54, 2729–2747.

Hop, H., Gjøsæter, H., 2013. Polar cod (*Boreogadus saida*) and capelin (*Mallotus villosus*) as key species in marine food webs of the Arctic and the Barents Sea. Mar. Biol. Res. 9 (9), 878–894.

Hunt Jr., G.L., Blanchard, A.L., Boveng, P., Dalpadado, P., Drinkwater, K.F., Eisner, L., Hopcroft, R.R., Kovacs, K.M., Norcross, B.L., Renaud, P., Reigstad, M., Renner, M., Skjoldal, H.R., Whitehouse, A., Woodgate, R.A., 2013. The Barents and Chukchi Seas: Comparison of two Arctic shelf ecosystems. J. Mar. Syst. 109–110, 43–68.

Huse, G., Ellingsen, I., 2008. Capelin migrations and climate change–a modelling analysis. Clim. Change 87 (1), 177–197.

Ingvaldsen, R.B., Gjøsæter, H., 2013. Responses in spatial distribution of Barents Sea capelin to changes in stock size, ocean temperature and ice cover. Mar. Biol. Res. 9 (9), 867–877. https://doi.org/10.1080/17451000.2013.775450.

Ingvaldsen, R., Loeng, H., Ottersen, G., Ådlandsvik, B., 2003. Climate variability in the Barents Sea during the 20th century with focus on the 1990s. ICES Marine Science Symposium 219, 160–168.

Ingvaldsen, R., Asplin, L., Loeng, H., 2004. Velocity field of the western entrance to the Barents Sea. J. Geophys. Res. 109, C03021. https://doi.org/10.1029/2003JC001811.

Ingvaldsen, R.B., Assmann, K.M., Primicerio, R., Fossheim, M., Polyakov, I.V., Dolgov, A. V., 2021. Physical manifestations and ecological implications of Arctic Atlantification. Nat. Rev. Earth & Environ. 2 (12), 874–889. https://doi.org/10.1038/s43017-021-00228- x.

Jakobsen, T., Ozhigin, V.K., 2011. The Barents Sea – ecosystem, resources, management. Half a century of Russian-Norwegian cooperation. Tapir academic press, Trondheim. 825 pp.

Jansen, T., Post, S., Kristiansen, T., Óskarsson, G.J., Boje, J., MacKenzie, B.R., Broberg, M., Siegstad, H., 2016. Ocean warming expands habitat of a rich natural resource and benefits a national economy. Ecol. Appl. 26 (7), 2021–2032.

Ji, R., Ashjian, C.J., Campbell, R.G., Chen, C., Gao, G., Davis, C.S., Cowles, G.W., Beardsley, R.C., 2012. Life history and biogeography of *Calanus* copepods in the Arctic Ocean: An individual-based modeling study. Prog. Oceanogr. 96, 40–56. https://doi.org/10.1016/j.pocean.2011.10.001.

Johannesen, E., Ingvaldsen, R.B., Bogstad, B., Dalpadado, P., Eriksen, E., Gjøsæter, H., Knutsen, T., Skern-Mauritzen, M., Stiansen, J.E., 2012. Changes in Barents Sea ecosystem state, 1970–2009: climate fluctuations, human impact, and trophic interactions. ICES J. Mar. Sci. 69, 880–889.

Kvile, K.Ø., Dalpadado, P., Orlova, E., Stenseth, N.C., Stige, L.C., 2014. Temperature effects on *Calanus finmarchicus* vary in space, time and between developmental stages. Mar. Ecol. Prog. Ser. 517, 85–104.

Kvile, K.Ø., Fiksen, Ø., Prokopchuk, I., Opdal, A.F., 2017. Coupling survey data with drift model results suggests that local spawning is important for *Calanus finmarchicus* production in the Barents Sea. J. Mar. Syst. 165, 69–76.

Langbehn, T.J., Varpe, Ø., 2017. Sea-ice loss boosts visual search: Fish foraging and changing pelagic interactions in polar oceans. Glob. Change Biol. 23 (12), 5318–5330. https://doi.org/10.1111/gcb.13797.

Lind, S., Ingvaldsen, R., 2012. Variability and impacts of Atlantic Water entering the Barents Sea from the north. Deep Sea Res. Part I 62, 70–88.

Lind, S., Ingvaldsen, R.B., Furevik, T., 2016. Arctic layer salinity controls heat loss from deep Atlantic layer in seasonally ice-covered areas of the Barents Sea. Geophys. Res. Lett. 43 (10), 5233–5242.

Loeng, H., 1991. Features of the oceanographic conditions of the Barents Sea. Polar Res. 10, 5–18.

Melle, W., Skjoldal, H.R., 1998. Reproduction and development of *Calanus finmarchicus*, *C. glacialis* and *C. hyperboreus* in the Barents Sea. Mar. Ecol. Prog. Ser. 169, 211–228.

Melle, W., Ellertsen, B., Skjoldal, H.R., 2004. Zooplankton: the link to higher trophic levels. In: Skjoldal, H.R. (Ed.), The Norwegian Sea Ecosystem. Tapir, Trondheim, pp. 137–202.

Melle, W., Runge, J., Head, E., Plourde, S., Castellani, C., Licandro, P., Pierson, J., Jonasdottir, S., Johnson, C., Broms, C., Debes, H., Falkenhaug, T., Gaard, E., Gislason, A., Heath, M., Niehoff, B., Nielsen, T.G., Pepin, P., Stenevik, E.K., Chust, G., 2014. The North Atlantic Ocean as habitat for *Calanus finmarchicus*: environmental factors and life history traits. Prog. Oceanogr. 129, 244–284.

Michalsen, K., Dalpadado, P., Eriksen, E., Gjøsæter, H., Ingvaldsen, R.B., Johannesen, E., Jørgensen, L.L., Knutsen, T., Prozorkevich, D., Skern-Mauritzen, M., 2013. Marine living resources of the Barents Sea - Ecosystem understanding and monitoring in a climate change perspective. Mar. Biol. Res. 9 (9), 932–947.

Nøttestad, L., Utne, K.R., Óskarsson, G.J., Jónsson, S.Þ., Jacobsen, J.A., Tangen, Ø., Anthonypillai, V., Aanes, S., Vølstad, J.H., Bernasconi, M., Debes, H., Smith, L., Sveinbjörnsson, S., Holst, J.C., Jansen, T., Slotte, A., 2016. Quantifying changes in abundance, biomass, and spatial distribution of Northeast Atlantic mackerel (*Scomber scombrus*) in the Nordic seas from 2007 to 2014. ICES J. Mar. Sci. 73 (2), 359–373.

Onarheim, I.H., Eldevik, T., Smedsrud, L.H., Stroeve, J.C., 2018. Seasonal and regional manifestation of Arctic sea ice loss. J. Clim. 31 (12), 4917–4932.

Orlova, E.L., Rudneva, G.B., Renaud, P.E., Eiane, K., Todd, P.A., Savinov, V., Yurko, A.S., 2010. Climate impacts on feeding and condition of capelin *Mallotus villosus* in the Barents Sea: evidence and mechanisms from a 30 year data set. Aquatic Biology 10 (2), 105–118.

Østvedt, O.-J., 1955. Zooplankton investigations from weathership 'M' in the Norwegian Sea, 1948–49. Hvalrådets Skrifter 40, 1–93.

Ottersen, G., Stenseth, N.C., 2001. Atlantic climate governs oceanographic and ecological variability in the Barents Sea. Limnol. Oceanogr. 46 (7), 1774–1780.

Ozhigin, V., Luka, G., 1985. Some peculiarities of capelin migrations depending on thermal conditions in the Barents Sea. In: Gjøsæter, H. (Ed.), Proceedings of the Soviet-Norwegian Symposium on the Barents Sea Capelin. Institute of Marine Research, Bergen, Norway, 1985, pp. 135–147.

Ozhigin, V., Ingvaldsen, R.B., Loeng, H., Boitsov, V., Karsakov, A., 2011. Introduction to the Barents Sea. In: Jakobsen, T., Ozhigin, V. (Eds.), The Barents Sea – Ecosystem, Resources, Management. Half a Century of Russian-Norwegian Cooperation. Tapir Academic Press, Trondheim, Norway, pp. 39–76.

Quadfasel, D., Rudels, B., Selchow, S., 1992. The Central Bank vortex in the Barents Sea: water mass transformation and circulation. ICES Marine Science Symposium 195, 40–51.

Rudels, B., 1989. Mixing processes in the northern Barents Sea. Rapport et Procès-verbaux de Réunions, Conseil Permanent International pour l'Exploration de la Mer 188, 36–48.

Rudels, B., 2021. The Physical Oceanography of the Arctic Mediterranean Sea: Explorations, Observations, Interpretations. Elsevier.

Sakshaug, E., Skjoldal, H.R., 1989. Life at the ice edge. Ambio 18, 60–67.

Skagseth, Ø., 2018. Hydrography in the Barents Sea from autumn cruises 1970-2016 by TIBIA subareas. In: Interim Report of the Working Group on the Integrated Assessments of the Barents Sea (WGIBAR). WGIBAR 2018 REPORT 9-12 March 2018. Tromsø, Norway. ICES CM 2018/IEASG:04, pp. 20-31.

Skagseth, Ø., Furevik, T., Ingvaldsen, R., Loeng, H., Mork, K.A., Orvik, K.A., Ozhigin, V., 2008. Volume and heat transports to the Arctic Ocean via the Norwegian and Barents Seas. In: Dickson, R., Meincke, J., Rhines, P. (Eds.), Arctic – Subarctic Ocean Fluxes: Defining the Role of the Northern Seas in Climate. Springer, New York, pp. 45–64.

Skagseth, Ø., Eldevik, T., Årthun, M., Asbjørnsen, H., Lien, V.S., Smedsrud, L.H., 2020. Reduced efficiency of the Barents Sea cooling machine. Nat. Clim. Change 10, 661–666. https://doi.org/10.1038/s41558-020-0772-6.

Skaret, G., Dalpadado, P., Hjøllo, S.S., Skogen, M.D., Strand, E., 2014. *Calanus finmarchicus* abundance, production and population dynamics in the Barents Sea in a future climate. Prog. Oceanogr. 125, 26–39.

Skjoldal, H.R., 2021. Species composition of three size fractions of zooplankton used in routine monitoring of the Barents Sea ecosystem. J. Plankton Res. 43 (5), 762–772.

Skjoldal, H.R. (Ed.), 2022. Ecosystem assessment of the Central Arctic Ocean: description of the ecosystem. Report from ICES/PICES/PAME Working Group on Integrated Ecosystem Assessment of the Central Arctic Ocean. ICES Cooperative Research Report 355, 341–pp. https://doi.org/10.17895/ices.pub.20191787.

Skjoldal, H.R., Rey, F., 1989. Pelagic production and variability of the Barents Sea ecosystem. In: Sherman, K., Alexander, L.M. (Eds.), Biomass Yields and Geography of Large Marine Ecosystems. AAAS Selected Symposium, 111. Westview Press, Inc., Colorado, USA, pp. 241–286.

Skjoldal, H.R., Hassel, A., Rey, F., Loeng, H., 1987. Spring phytoplankton development and zooplankton reproduction in the central Barents Sea in the period 1979–1984. In: Loeng, H. (Ed.), The Effect of Oceanographic Conditions on Distribution and Population Dynamics of Commercial Fish Stocks in the Barents Sea. Proceedings of the Third Soviet–Norwegian Symposium, Murmansk, 26–28 May 1986, pp. 59–89.

Skjoldal, H.R., Gjøsæter, H., Loeng, H., 1992. The Barents Sea ecosystem in the 1980s — ocean climate, plankton, and capelin growth. ICES Marine Science Symposium 195, 278–290.

Skjoldal, H.R., Wiebe, P.H., Postel, L., Knutsen, T., Kaartvedt, S., Sameoto, D.D., 2013. Intercomparison of zooplankton (net) sampling systems: Results from the ICES/GLOBEC sea-going workshop. Prog. Oceanogr. 108, 1–42.

Skjoldal, H.R., Dalpadado, P., Aarflot, J.M., Bagøien, E., Dolgov, A., Prokopchuk, I., and Reeves, M., 2018. New time-series of zooplankton biomass in the Barents Sea 1989–2016. In: Interim Report of the Working Group on the Integrated Assessments of the Barents Sea (WGIBAR). WGIBAR 2018 Report, 9-12 March 2018. Tromsø, Norway. ICES CM 2018/IEASG:04, pp. 32-54.

Skjoldal, H.R., Prokopchuk, I., Bagøien, E., Dalpadado, P., Nesterova, V., Rønning, J., Knutsen, T., 2019. Comparison of Juday and WP2 nets used in joint Norwegian-Russian monitoring of zooplankton in the Barents Sea. J. Plankton Res. 41 (5), 759–769. https://doi.org/10.1093/plankt/fbz054.

Skjoldal, H.R., Aarflot, J.M., Bagøien, E., Skagseth, Ø., Rønning, J., Lien, V.S., 2021. Seasonal and interannual variability in abundance and population development of *Calanus finmarchicus* at the western entrance to the Barents Sea, 1995–2019. Prog. Oceanogr. 195, 102574 https://doi.org/10.1016/j.pocean.2021.102574.

Slagstad, D., Ellingsen, I.H., Wassmann, P., 2011. Evaluating primary and secondary production in an Arctic Ocean void of summer sea ice: an experimental simulation approach. Prog. Oceanogr. 90 (1–4), 117–131.

Smedsrud, L.H., Muilwijk, M., Brakstad, A., Madonna, E., Lauvset, S.K., Spensberger, C., Born, A., Eldevik, T., Drange, H., Jeansson, E., Li, C., Olsen, A., Skagseth, Ø., Slater, D.A., Straneo, F., Våge, K., Årthun, M., 2022. Nordic Seas heat loss, Atlantic inflow, and Arctic sea ice cover over the last century. Rev. Geophys. 60 https://doi.org/10.1029/2020RG000725.

Søreide, J.E., Leu, E., Berge, J., Graeve, M., Falk-Petersen, S., 2010. Timing of blooms, algal food quality and *Calanus glacialis* reproduction and growth in a changing Arctic. Glob. Change Biol. 16 (11), 3154–3163. https://doi.org/10.1111/j.1365-2486.2010.02175.x.

Stige, L.C., Dalpadado, P., Orlova, E., Boulay, A.C., Durant, J.M., Ottersen, G., Stenseth, N.C., 2014. Spatiotemporal statistical analyses reveal predator-driven zooplankton fluctuations in the Barents Sea. Prog. Oceanogr. 120, 243–253. https://doi.org/10.1016/j.pocean.2013.09.006.

Strand, E., Bagøien, E., Edwards, M., Broms, C., Klevjer, T., 2020. Spatial distributions and seasonality of four *Calanus* species in the Northeast Atlantic. Prog. Oceanogr. 185, 102344.

Sundby, S., 2000. Recruitment of Atlantic cod stocks in relation to temperature and advection of copepod populations. Sarsia 85, 277–298.

Tande, K.S., 1991. *Calanus* in North Norwegian fjords and in the Barents Sea. Polar Res. 10 (2), 389–408.

Tarling, G.A., Freer, J.J., Banas, N.S., Belcher, A., Blackwell, M., Castellani, C., Cook, K. B., Cottier, F.R., Daase, M., Johnson, M.L., Last, K.S., Lindeque, P.K., Mayor, D.J., Mitchell, E., Parry, H.E., Speirs, D.C., Stowasser, G., Wootton, M., 2022. Can a key boreal *Calanus* copepod species now complete its life-cycle in the Arctic? Evidence and implications for Arctic food-webs. Ambio 51 (2), 333–344.

Tranter, D.J. (Ed.), 1968. Reviews on zooplankton sampling methods. In: Zooplankton Sampling, Part I. Monographs on Oceanographic Methodology Vol. 2. Unesco Press, UNESCO, Paris, pp. 11–144.

Wassmann, P., Reigstad, M., Haug, T., Rudels, B., Carroll, M.L., Hop, H., Gabrielsen, G. W., Falk-Petersen, S., Denisenko, S.G., Arashkevich, E., Slagstad, D., Pavlova, O., 2006. Food webs and carbon flux in the Barents Sea. Prog. Oceanogr. 71 (2-4), 232–287.

WGIBAR, 2017. Report of the Working Group on the Integrated Assessments of the Barents Sea. WGIBAR 2017 Report 16-18 March 2017, Murmansk, Russia. ICES CM 2017/SSGIEA:04. 186 pp.

WGIBAR, 2021. Working Group on the Integrated Assessments of the Barents Sea (WGIBAR). ICES Scientific Reports 3 (77), 236. https://doi.org/10.17895/ices.pub.8241.